



Atmospheric oxygen as a tracer for fossil fuel carbon dioxide: a sensitivity study in the UK

Hannah Chawner¹, Karina E. Adcock², Tim Arnold^{3,4}, Yuri Artioli⁵, Caroline Dylag³, Grant L. Forster^{2,6}, Anita Ganesan⁷, Heather Graven⁸, Gennadi Lessin⁵, Peter Levy⁹, Ingrid T. Luijkx¹⁰, Alistair Manning¹¹, Penelope A. Pickers², Chris Rennick³, Christian Rödenbeck¹², and Matthew Rigby¹

¹School of Chemistry, University of Bristol, Bristol, UK

²Centre for Ocean and Atmospheric Sciences, School of Environmental Sciences, University of East Anglia, Norwich, UK

³National Physical Laboratory, Teddington, UK

⁴School of Geosciences, University of Edinburgh, Edinburgh, UK

⁵Plymouth Marine Laboratory, Plymouth, UK

⁶National Centre for Atmospheric Sciences, University of East Anglia, UK

⁷School of Geographical Sciences, University of Bristol, Bristol, UK

⁸Department of Physics, Imperial College London, London, UK

⁹Centre for Ecology and Hydrology, Edinburgh, UK

¹⁰Meteorology and Air Quality, Wageningen University and Research, Wageningen, the Netherlands

¹¹Hadley Centre, Met Office, Exeter, UK

¹²Max Planck Institute for Biogeochemistry, Germany

Correspondence: Hannah Chawner (hannah.chawner@bristol.ac.uk), Matt Rigby (matt.rigby@bristol.ac.uk)

Abstract. We investigate the use of oxygen (O₂) and carbon dioxide (CO₂) measurements for the estimation of the fossil fuel component of atmospheric CO₂ in the UK. Atmospheric potential oxygen (APO) – a tracer that combines O₂ and CO₂, minimising the influence of terrestrial biosphere fluxes – is simulated at three sites in the UK, two of which make atmospheric APO measurements. We present a set of model experiments that estimate the sensitivity of APO simulations to key inputs: 5 fluxes from the ocean, fossil fuel flux magnitude and distribution, the APO baseline, and the ratio of O₂ to CO₂ fluxes from fossil fuel combustion and the terrestrial biosphere. To estimate the influence of uncertainties in ocean fluxes, we compared three ocean O₂ flux estimates, from the NEMO–ERSEM and ECCO-Darwin ocean models, and the Jena CarboScope APO inversion. The sensitivity of APO to fossil fuel emission magnitudes and to terrestrial biosphere and fossil fuel exchange ratios was investigated through Monte Carlo sampling within literature uncertainty ranges, and by comparing different inventory 10 estimates. Of the factors that could potentially compromise APO-derived fossil fuel CO₂ estimates, we find that the ocean O₂ flux estimate has the largest overall influence at the three sites in the UK. At times, this influence is comparable to the contribution to APO of simulated fossil fuel CO₂. We find that simulations using different ocean fluxes differ from each other substantially, with no single model estimate, or a simulation with zero ocean flux, providing a significantly closer fit to the observations. Furthermore, the uncertainty in the ocean contribution to APO could lead to uncertainty in defining an 15 appropriate regional background from the data. Our findings suggest that the contribution of non-terrestrial sources need to be well accounted for, in order to reduce their potential influence on inferred fossil fuel CO₂.



1 Introduction

Variations in atmospheric carbon dioxide (CO_2) concentrations are due to atmospheric transport and the influence of fluxes from the terrestrial biosphere, the ocean and human activities. With the ultimate aim of evaluating national emission estimates, a major goal of several recent studies has been the isolation of only those variations due to anthropogenic fossil fuel CO_2 emissions. Radiocarbon, ^{14}C , has been widely used as a tracer for this purpose (e.g. Levin et al., 2003; Graven et al., 2009, 2018; Wenger et al., 2019), as fossil fuel emissions are fully depleted in ^{14}C , providing a signature with which to discriminate fossil fuel emissions from other sources and sinks. However, such measurements are expensive, they cannot be made continuously to the required precision, and in some regions there may be significant interference of ^{14}C emission from gas-cooled nuclear power stations (Graven and Gruber, 2011; Bozhinova et al., 2016; Wenger et al., 2019). An alternative tracer is carbon monoxide (CO), which is released by incomplete combustion. Measurements of CO are much less expensive than those of ^{14}C and can be made continuously (e.g. Andrews et al., 2014; Levin and Karstens, 2007; Levin et al., 2020). However, there is large uncertainty in both the ratio of CO to CO_2 emissions from fossil fuel combustion, and the CO flux from non-fossil fuel sources and sinks.

Pickers (2016) and Pickers et al. (2022) show that oxygen (O_2) and CO_2 measurements, combined into Atmospheric Potential Oxygen (APO) (Stephens et al., 1998), can be used as a novel tracer for fossil fuel derived CO_2 . In their study, Pickers et al. (2022) show that their APO-derived CO_2 emission changes during the COVID-19 lockdowns in the UK correspond well to the changes found from bottom-up inventories. Their method, combining observations and machine-learning techniques, shows the potential of APO as a fossil fuel CO_2 (ff CO_2) tracer. The basis of this method is that the ratio of O_2 to CO_2 fluxes from the terrestrial biosphere, which are by definition removed from the O_2 signal through the use of the APO tracer (Stephens et al., 1998), is relatively well constrained and invariant in space and time. For the land-based sources, O_2 and CO_2 fluxes to the atmosphere from photosynthesis, respiration, and combustion are strongly anti-correlated: CO_2 is taken up through photosynthesis whilst O_2 is released, and the reverse is true for respiration and combustion. When considering ocean fluxes, the situation is more complex, as differences in solubility (Keeling, 1988a) and carbonate chemistry (Keeling and Shertz, 1992; Keeling and Severinghaus, 2000) mean that the O_2 and CO_2 fluxes from the ocean are largely decoupled. However, previous work has indicated that the influence of ocean fluxes on the atmospheric ratio of O_2 to CO_2 is generally smaller than the influence of fossil fuel combustion on short timescales (Pickers, 2016; Pickers et al., 2017; Chevalier and WP4 CHE partners, 2021). Pickers et al. (2017) found short-term variability in APO, O_2 and CO_2 mole fractions with only very small magnitude from the ocean when taking ship measurements.

There have been a number of promising attempts to incorporate O_2 modelling as a tracer for ff CO_2 . Kuijpers et al. (2018) modelled O_2 for the autumn of 2015 for three sites in the UK and the Netherlands, finding good agreement with observations. APO modelling was investigated to derive European ff CO_2 fluxes by several groups within the CO_2 Human Emissions project (CHE, work package 4, Marshall et al., 2019; Chevalier and WP4 CHE partners, 2021). Comparing with results from $\Delta^{14}\text{CO}_2$ and CO modelling, they found that APO-derived ff CO_2 gave the strongest correlation to direct ff CO_2 models using STILT and TNO fluxes. The APO models were affected by oceanic fluxes at some coastal sites, although for most coastal sites the ocean influence, using ocean fluxes from NEMO - PlankTOM5, was considerably smaller than that of the ff CO_2 .



Two measurement sites equipped with high-frequency CO₂ and O₂ instruments have been established in the UK, one at Weybourne Atmospheric Observatory (WAO) in the East of England and one at Heathfield tower (HFD) in the South of England. In this paper, we perform simulations of CO₂ and O₂ focusing on these locations, along with a third site at Ridge Hill (RGL). Although O₂ measurements are not available from RGL, it is included to examine the modelled APO further inland.

55 We test the sensitivity of the APO simulation to changes in a set of uncertain model input parameters, to determine whether a robust tracer of national scale fossil fuel CO₂ can be derived.

1.1 Modelling Atmospheric Potential Oxygen

As O₂ is abundant in the atmosphere, dilution by trace gases can have a non-negligible effect on its mole fraction which may erroneously be attributed to an O₂ flux. To minimise this influence, oxygen measurements are commonly reported as a ratio
60 with respect to the atmospheric nitrogen mole fraction as $\delta(O_2/N_2)$ (Keeling and Shertz, 1992):

$$\delta(O_2/N_2) = \frac{(O_2/N_2)_{sample} - (O_2/N_2)_{reference}}{(O_2/N_2)_{reference}} \times 10^6 \quad (1)$$

where $(O_2/N_2)_{sample}$ is the O₂/N₂ ratio of a sample, and $(O_2/N_2)_{reference}$ is from a reference gas cylinder. $\delta(O_2/N_2)$ is expressed in per meg.

We can define the tracer APO(e.g. Stephens et al., 1998; Gruber et al., 2001; Battle et al., 2006) that is largely unaffected
65 by exchanges with the terrestrial biosphere, but sensitive to fossil fuel and ocean fluxes. This is a weighted combination of O₂ and CO₂ which isolates the oceanic and fossil fuel components:

$$APO = O_2 + \alpha_B \times (CO_2 - 350) \quad (2)$$

where APO is a mole fraction, α_B is the O₂:CO₂ exchange ratio for the land biosphere, O₂ and CO₂ are the atmospheric mole fractions of O₂ and CO₂ respectively, and 350 ($\mu\text{mol mol}^{-1}$) is an arbitrary reference.

70 Equations 1 and 2 can be combined, expressing APO in units of per meg (Stephens et al., 1998):

$$APO = \delta(O_2/N_2) + \left(\frac{\alpha_B}{S_{O_2}}\right) \times (CO_2 - 350) \quad (3)$$

where S_{O_2} is the standard mole fraction of O₂ in air, equal to 0.20946 (Machta and Hughes, 1970).

1.1.1 The regional contribution to atmospheric APO

The regional contribution of atmospheric APO can be estimated by combining the mole fraction contribution of O₂, CO₂, and
75 N₂. Following the derivation in Manning and Keeling (2006), the deviation of APO can be expressed as:

$$\Delta(\delta APO) = \frac{Z + (\alpha_F - \alpha_B)F + \alpha_B O}{S_{O_2}(1 - S_{O_2})} - \frac{N}{S_{N_2}} \quad (4)$$

$$= \frac{Z + F_O - \alpha_B F + \alpha_B O}{S_{O_2}(1 - S_{O_2})} - \frac{N}{S_{N_2}} \quad (5)$$



where Z and O respectively are the O_2 and CO_2 mole fraction contributions from the ocean; F and F_O are the contributions of CO_2 and O_2 respectively from fossil fuel combustion and cement production; N is the N_2 contribution; α_F and α_B are the fossil fuel and biospheric exchange ratios; and S_{N_2} is the mole fraction of N_2 in dry air, given as 0.78084 (Weast and Astle, 1982), where this and S_{O_2} are used to convert from units of ppm ($\mu\text{mol/mol}$) to per meg. A correction of $(1 - S_{O_2})$ accounts for dilution effects of O_2 (Kozlova et al., 2008).

When estimating the exchange of N_2 we need only to consider the ocean contribution as the other components are assumed to be negligible (Ciais et al., 2007). We assume a constant value for α_B for the UK of -1.07 ± 0.04 (Marshall et al., 2019; Pickers). α_F varies for different fuel types, having values of -1.17 for coal, -1.44 for oil, -1.95 for gas, and 0 for cement production (Keeling, 1988b; Steinbach et al., 2011), and can be estimated for the UK by combining fossil fuel emissions estimates and fuel usage statistics, as outlined in Section 2.2.2. Variations in α_F are not well studied or constrained, however we follow Jones et al. (2021) in assuming an uncertainty of ± 3 per cent.

2 Methodology

2.1 Observations

At both the measurement sites, WAO and HFD, atmospheric O_2 measurements are made using ‘Oxzilla’ lead fuel cell analysers (Sable Systems International Inc.) placed in series with non-dispersive infrared (NDIR) CO_2 ‘Ultramat 6E’ analysers (Siemens Corp.). The gas handling for each system is similar to that of Adcock et al. (in prep.), Pickers et al. (2017) and Stephens et al. (2007), to ensure stable pressures and flow rates are maintained and to avoid O_2/N_2 fractionation effects. A two-stage drying system (Wilson, 2013; Barningham, 2018; Adcock et al., in prep.) reduces the dew point of the sample air to approximately -90°C . Calibration gases, consisting of secondary standards that are stored horizontally in thermally insulated enclosures, are used to characterise analyser responses on the WMO CO_2 scale maintained by NOAA and the Scripps Institution of Oceanography scale for O_2 , by employing routines and protocols similar to those of Kozlova and Manning (2009).

Weybourne Atmospheric Observatory (WAO; <https://weybourne.uea.ac.uk/>) is a coastal measurement station in Norfolk, in the east of England ($52^\circ 57' 02''\text{N}$, $1^\circ 07' 19''\text{E}$) which has been routinely sampling CO_2 and O_2 since May 2010. Established in 1992, WAO is a Global Atmospheric Watch (GAW) Regional station, an National Centre for Atmospheric Sciences (NCAS) Atmospheric Measurement Facility (AMF), and an Integrated Carbon Observation System (ICOS) Class 2 station. Air is alternately sampled from two identical aspirated inlets at 15 magl (Blaine et al., 2006).

Heathfield (HFD) is a tall-tower measurement site that is part of the UK Deriving Emissions linked to Climate Change (DECC) network (Stanley et al., 2018) which has been sampling CO_2 and O_2 since June 2021. The site is in an agricultural area in the south of England ($50^\circ 58' 36.3''\text{N}$, $0^\circ 13' 49.728''\text{E}$), around 25 km north of the English Channel. Air is alternately sampled from two identical aspirated inlets (Blaine et al., 2006) at 100 magl.

Ridge Hill is also a tall-tower measurement site in the UK DECC network in Herefordshire ($51^\circ 59' 50.766''\text{N}$, $2^\circ 32' 23.64''\text{W}$). Although CO_2 is sampled here, O_2 is not, yet we include this site in the analysis to test the model at a more inland UK site.



110 The repeatability of the O₂ measurements from Weybourne, which is determined from regular measurements of a target tank,
typically ranges from 1.68 ± 1.09 per meg to 3.31 ± 5.46 per meg (Adcock et al, in prep). This exceeds WMO repeatability goals
(WMO, 2019) for O₂, but is nevertheless amongst the most precise globally. The repeatability is calculated using the method
explained in Pickers et al. (2017) and is reported with $\pm 1\sigma$ uncertainty to represent how the measurement system repeatability
varies over time. During the period February to November 2015, the O₂ measurement repeatability was significantly larger
115 (10.71 ± 10.45) than usual, caused by poor performance of the Oxzilla analyser. As described in Section 2.2, we model 2015 as
it is the most recent year for which outputs exist for all of the ocean models used. This larger repeatability does not significantly
affect the accuracy of the O₂ measurements, but does compromise the detection limit, meaning that smaller synoptic variations
in APO (<10–20 per meg) may be masked during this period by the measurement imprecision. CO₂ repeatability was not
affected, and is 0.005 ± 0.023 ppm on average at Weybourne, calculated from over 8000 target tank measurements made from
120 2010–2021.

2.2 Modelling APO

We use a Lagrangian particle dispersion model (LPDM) to simulate APO at the measurement sites in the south of the UK. The
key components of our simulation are the LPDM “footprints”, a set of flux estimates, and boundary conditions at the edge of
our domain. The following sections outline how each component was produced and used.

125 For our analysis we focus on the year 2015, chosen because time-resolved ocean model outputs are available for all ocean
models considered here, described in Section 2.2.2. Weybourne measurements are available for 2015 and are compared to the
simulation in Section 3. Heathfield observations are only available from June 2021, when time-resolved ocean fluxes are not
available, so model outputs, derived using climatological fluxes, are compared to the observational data for this site and shown
in the Supplement. Simulations at Ridge Hill are shown in the Supplement.

130 We also model the total CO₂ and O₂ mole fraction at Weybourne to compare the correlations with those observations to the
equivalent for APO.

2.2.1 The Atmospheric Model

Simulations of atmospheric transport and dispersion are carried out using the Numerical Atmospheric-dispersion Modelling
Environment (NAME III, version 7.2), the UK Met Office’s LPDM (Jones et al., 2007). NAME was run in time-reversed
135 mode, in which we tracked thousands of model particles back in time for 30 days from observation sites (see e.g. Manning
et al., 2011). The motion of hypothetical “particles” is simulated based on meteorological fields from the Met Office Unified
Model analyses (Cullen, 1993). The “footprint” of each measurement was estimated by recording locations and times at which
particles interacted with the Earth’s surface (defined as being the lowest 40 m of the atmosphere in this case). These footprints
define the sensitivity of mole fractions at a measurement site to the flux from each grid cell in the domain. Our domain covered
140 most of Europe, the east coast of North and Central America, and North Africa, extending across the longitude/latitude range:
 $10.729 - 79.057^\circ\text{N}$ and $97.9^\circ\text{W} - 39.38^\circ\text{E}$ (shown in Supplementary Figure S1). The footprints have the resolution 0.234° by
 0.352° (roughly 25 km by 25 km over the UK).

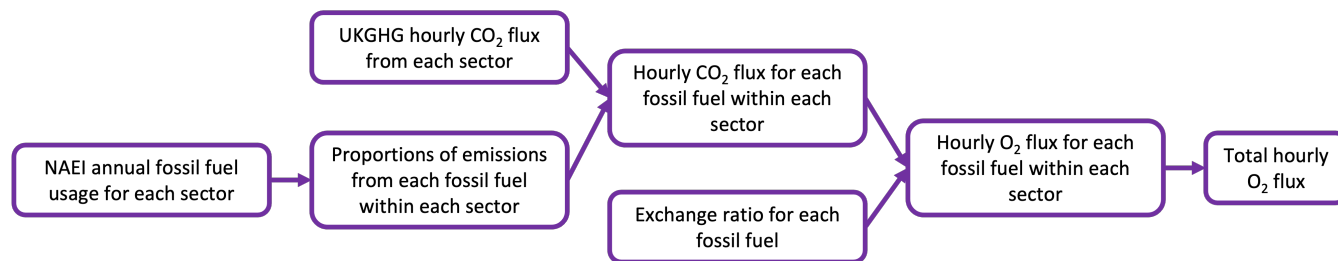


Figure 1. Calculation of UK fossil fuel O₂ fluxes from CO₂ flux estimates and fuel usage statistics from the UK National Atmospheric Emissions Inventory (NAEI), where flux estimates are downscaled to an hourly resolution using UKGHG (White et al., 2019).

The NAME footprints used for this study are disaggregated in time with the method described by White et al. (2019). To account for the influence on the mole fractions of rapid variations in CO₂ flux, footprints are generated hourly for the 24 hours preceding a simulated data point. Time-integrated footprints are then used for the remaining 29 days of the simulation. The modelled regional contribution to the mole fraction of a species, Y_t , at a time-step, t , can then be estimated by combining the flux field with the high-time-resolution NAME footprint, as shown by equation 6 (White et al., 2019):

$$Y_t = \sum_{h=0}^H \sum_{j=0}^n f p_{t-h,j} \times q_{t-h,j} + \sum_{j=0}^n f p_{remainder_j} \times q_{month_j} \quad (6)$$

where H is the number of hours back in time over which the footprint is disaggregated, for which we use 24; h is the number of hours back in time before the particle release time, t ; j is the grid cell and n is the maximum number of grid cells; $f p_{t-h,j}$ is one grid cell of the footprint for that time; $q_{t-h,j}$ is one grid cell of the flux field; $f p_{remainder_j}$ is the remaining 29-day footprint; and q_{month_j} is the monthly average flux for the grid cell (by calendar month). White et al. (2019) discusses this method in more detail, including the effects of varying the level of time-disaggregation of the footprint, H .

2.2.2 Flux products

We model the regional contribution to APO separately for each of the components of Equation 5 (Z , F_O , F , O), using Equation 6 to combine the flux estimates and NAME footprints. Here we describe how the fluxes for each component are estimated.

Anthropogenic CO₂ flux estimates for the UK are taken from the UK National Atmospheric Emissions Inventory (NAEI), where estimates at a downscaled hourly resolution are derived using the UKGHG model (White et al., 2019). Outside of the UK, anthropogenic flux estimates from EDGAR (Emissions Database for Global Atmospheric Research) are used. As NAEI includes the anthropogenic CO₂ flux estimates from both fossil fuel and non-fossil fuel sources (e.g. peat and biomass), we use the method described in Figure 1 and Equations 7 and 8 to remove emissions associated with non-fossil fuel sources, and thus estimate the fossil fuel UK CO₂ and O₂ flux:

$$CO_{2ff} = \sum_s \sum_e CO_{2s} R_{se} \quad (7)$$



$$165 \quad O_{2ff} = \sum_s \sum_e CO_{2s} R_{se} \alpha_{fe} \quad (8)$$

where s is the SNAP sector (Selected Nomenclature for reporting of Air Pollutants, see e.g. Tsagatakis et al., 2022), e is the fuel or source type (coal, oil, gas, non-combustion, or cement production), CO_{2s} is the CO_2 flux for the sector, R_{se} is the proportion of CO_2 emissions within the SNAP sector associated with the fuel type, and α_{fe} is the fossil fuel exchange ratio for the fuel type. We use NAEI statistics of the annual fuel usage for each SNAP sector¹ to determine R_{se} , assuming that the ratio of fuels used within each sector is constant throughout the year. When determining the fuel type associated with NAEI emissions estimates we follow the assumptions given by Jones et al. (2021), that emissions from the non-energy use of fuels and solvent sector relate to non-combustion use of oil, and emissions from the production of non-metallic minerals relate to cement clinker production. Using the exchange ratio for each fuel, α_{fe} , we then convert from CO_2 to O_2 flux for each fuel within each sector, and take the sum to give the total hourly O_2 flux throughout the year. The O_2 flux from outside of the UK is estimated using EDGAR CO_2 fields and α_F estimates from GridFED (Jones et al., 2021).

We compare ocean CO_2 and O_2 fluxes derived from NEMO – ERSEM simulations (NE, Butenschön et al., 2016; Madec and NEMO System Team, 2022), the ECCO – Darwin model (ED, Carroll et al., 2020) and the Jena CarboScope APO inversion (JC, Rödenbeck et al., 2008), as well as a model with ocean fluxes excluded. All of the ocean fluxes have daily time resolution and raw spatial resolutions of $0.199^\circ \times 0.333^\circ$, $2.0^\circ \times 2.5^\circ$, and $0.066^\circ \times 0.110^\circ$ for ED, JC, and NE respectively, which are regridded to match the NAME spatial resolution for our analysis.

ED determines ocean-atmosphere transfer of O_2 and CO_2 by combining the CO_2 partial pressure difference across the air-sea interface with the relationship between wind speed and gas transfer, as described by Wanninkhof (1992). The Darwin Project biogeochemical model resolves the cycling of CO_2 and O_2 and its ocean ecology includes phytoplankton and zooplankton (Brix et al., 2015; Carroll et al., 2020). JC estimates CO_2 and APO fluxes using a Bayesian atmospheric inversion and measurements from 23 CO_2 stations and up to 10 O_2 stations (including Weybourne, Rödenbeck et al., 2003, 2008, 2018). For the JC APO inversion oceanic CO_2 fluxes are estimated from the interpolation of pCO_2 data, Air-sea fluxes of O_2 and CO_2 in NE are calculated starting from the gradient of those gases between the atmosphere and the water and using Nightingale et al. (2000) to estimate the gas transfer coefficient. The concentration of O_2 and CO_2 in the water are the results of dynamical processes in the ecosystem represented in the model, and in particular photosynthesis from phytoplankton and respiration of all planktonic community as well as benthic organisms. More details on the dynamics of these gases can be found in Butenschön et al. (2016). For all of our APO models we use a nitrogen flux field estimated from NEMO heat fluxes by Equation 9:

$$190 \quad q_{ocean_N} = -\frac{dC_{eq}}{dT} \frac{\dot{Q}}{C_p} \quad (9)$$

¹<https://naei.beis.gov.uk/data/data-selector>



where dC_{eq}/dT is the temperature derivative of the solubility, \dot{Q} is the ocean heat flux (positive for transfer from the ocean to the atmosphere), and C_p is the heat capacity of seawater (Keeling et al., 1993). dC_{eq}/dT is estimated using:

$$195 \quad \ln C = A_0 + A_1 T_S + A_2 T_S^2 + A_3 T_S^3 + S(B_0 + B_1 T_S + B_2 T_S^2) \quad (10)$$

with

$$T_S = \ln\left(\frac{571.3 - T}{T}\right) \quad (11)$$

where C is the gas concentration, T is the temperature (K), S is the salinity and the A and B coefficients are defined in Hamme (2004). The surface heat flux is calculated by NEMO as the balance between the non-solar heat (sum of sensible, latent and
200 long wave heat fluxes) and the incoming solar radiation (Madec and NEMO System Team, 2022). Both the ocean temperature and salinity are derived from the NE simulation.

When modelling CO_2 and O_2 mole fractions separately, we must include a terrestrial flux component. For this we use CO_2 flux estimates from the Organising Carbon and Hydrology In Dynamic Ecosystems (ORCHIDEE, Krinner et al., 2005) model. ORCHIDEE is a dynamic vegetation model which simulates the principal biospheric processes influencing the global carbon
205 cycle, including photosynthesis, autotrophic and heterotrophic respiration. To estimate the terrestrial O_2 flux we multiply the CO_2 flux by α_B , which we assumed is equal to 1.07 ± 0.04 (see Section 1.1).

2.2.3 APO boundary conditions

With the method of Lunt et al. (2016), we model the contribution from the boundary conditions at the edge of our domain using global atmospheric fields of APO mixing ratios from the JC global APO inversion (Rödenbeck et al., 2008, version
210 apo99X_WAO_v2021). These boundary conditions are propagated to the measurement site by tracking the location at which NAME model particles leave the domain, thus providing a baseline estimate at the site. The baseline estimated from the boundary conditions is adjusted for consistency with the observations. To do this, we adjust the JC background for each month such that the simulated APO during periods of minimal terrestrial influence (defined as the 90 percentile of APO in a simulation with no ocean fluxes) are consistent with the observations at the same times. The original and adjusted JC backgrounds are
215 shown in Figure S2 in the Supplement.

2.3 Sensitivity experiments

Model simulations of APO are sensitive to uncertainties in several inputs of Equation 5. In this section, we outline how we investigate the sensitivities to the biospheric and anthropogenic exchange ratios (α_B and α_F), ocean fluxes, fossil fuel CO_2 emissions, baseline, and atmospheric model.

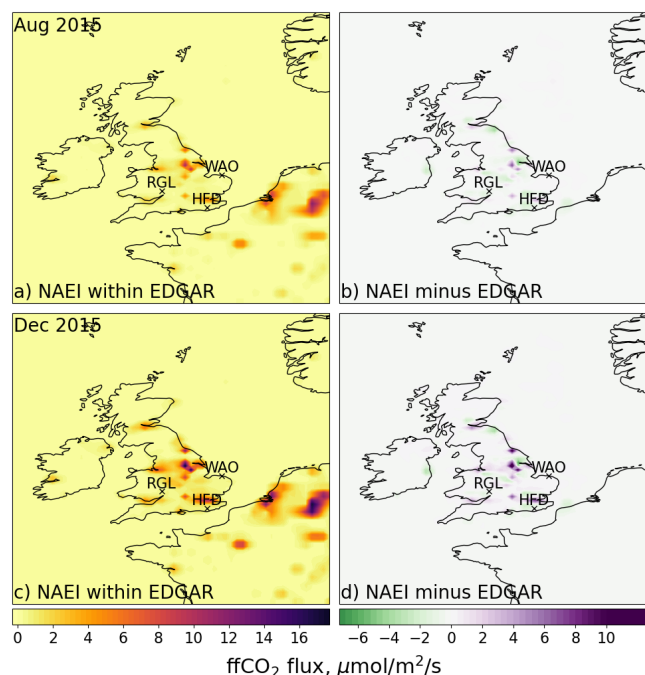


Figure 2. The ffCO_2 flux estimated by NAEI, embedded in EDGAR (panels *a* and *c*), and the difference between the NAEI and the EDGAR fields (panels *b* and *d*) for August (panels *a* and *b*) and December 2015 (panels *c* and *d*). By definition panels *b* and *d* are zero outside of the UK. The crosses show the locations of the sites included in this study: HFD, RGL, and WAO.

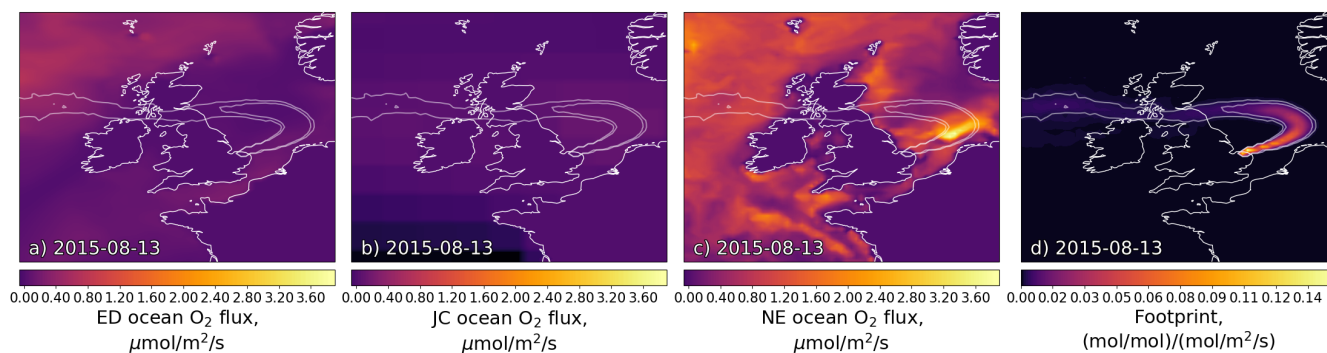


Figure 3. The daily mean O_2 ocean flux fields from the ED model (panel *a*), the JC Inversion (panel *b*) and NE model (panel *c*), and the NAME footprint (panel *d*) on the 13/08/2015, at a time at which the ED and NE ocean fluxes dominate the simulated APO and when there is a large difference between the estimated O_2 contribution from the three flux estimates. The flux fields have the 0.002 and 0.005 $(\text{mol/mol})/(\text{mol/m}^2/\text{s})$ footprint contour overlaid.



220 2.3.1 Sensitivity to the exchange ratios: α_B and α_F

To investigate our sensitivity to α_B and α_F in Equation 5 we employ a Monte Carlo method, randomly generating a value for each from a Gaussian distribution with a standard deviation of 0.04 mol/mol (Marshall et al., 2019) and 3 per cent (Jones et al., 2021) for α_B and α_F respectively. Doing so, we generate 1000 values for the APO time-series.

As α_F varies for different fuels we must take this into account when studying the sensitivity to α_F . As described in section 2.2.2, the fossil fuel O₂ flux for each sector is calculated using α_F based on the proportion of fuels consumed within that sector. We therefore initially investigate the sector-wise sensitivity of the O₂ flux to α_F for each fossil fuel: coal, oil, and gas. Then we combine this information to determine the overall sensitivity of the fossil fuel O₂ flux and the APO simulation to α_F .

2.3.2 Sensitivity to fossil fuel flux magnitude and distribution

The modelled APO is dependent on fossil fuel flux estimates, and here we study the sensitivity of the modelled fossil fuel contribution to the atmospheric concentration of CO₂ and O₂. We first examine how the APO model may be affected by estimates of the distribution of ffCO₂ emissions. As shown in Figure 2, there are differences in the distribution of CO₂ flux estimated by two different CO₂ inventories: NAEI and EDGAR, and we can compare the APO model using these to investigate this effect. As discussed in Section 2.2, our APO model uses NAEI ffCO₂ emissions estimates for the UK which are embedded in those of EDGAR, as well as NAEI fuel usage statistics to calculate ffO₂ uptake. Here we compare with EDGAR CO₂ emissions, using the GridFED estimates of α_F to estimate ffO₂.

We further investigate the sensitivity of the model to the magnitude of ffCO₂ estimates using a Monte Carlo ensemble in which the overall CO₂ flux in the entire domain is allowed to vary by $\pm 10\%$ (considerably larger than the difference between EDGAR and the NAEI, which is approximately 0.7%, but chosen so that the effect on APO can be readily identified).

2.3.3 Sensitivity to ocean flux

Figure 3 shows the ocean flux fields from the ED and NE models and the JC inversion. For illustration, this figure is shown for a period (13th August 2015) when the footprint for WAO is predominantly across the ocean. On this date, and in general, there is a much larger flux in coastal regions in the NE ocean model compared with both the ED and JC estimates. Unlike exchange ratios, the sensitivity of simulated APO to ocean fluxes cannot readily be described by an uncertainty on a single parameter. Therefore, to examine the sensitivity to this term we produce APO timeseries using the three different flux estimates such that we can qualitatively compare the effect on APO magnitude and variability, and compare the correlation of each model with the observations. We also produce a timeseries with the ocean component excluded to examine whether the fit to the observations can be improved by assuming a negligible ocean contribution.

2.3.4 Sensitivity to the background estimate

We study the effects of the background APO estimate on our simulations. The background represents the APO variability that is representative of the well-mixed atmosphere at the UK's latitude, excluding local influences. To do so, here we compare the



modelled $\Delta(\delta APO)$ (calculated using equation 5) with background-subtracted observations at Weybourne throughout 2015. We compare two methods to subtract the background from the observations. First we estimate a baseline from the APO observations using the ‘REBS’ statistical fitting routine (Robust Extraction of Baseline Signal, Ruckstuhl et al., 2012; Pickers et al., 2022) with a span value of 0.03, equivalent to a smoothing window of approximately one week. This smoothing window
255 was thought to be the most appropriate for incorporating wider-scale APO signals from outside Europe into the background term while simultaneously excluding local influences. For our second background subtraction we use the JC background estimate, estimated from boundary conditions propagated to the measurement site using NAME (Section 2.2.3). A monthly adjustment is made to the JC background to account for offsets observed in some months, as described in Section 2.2.3. This gives us two estimates of observation-derived $ffCO_2$, using which we can compare the background subtraction method.

260 These background estimates are inherently different: for example the REBS baseline incorporates regional ocean seasonality whereas the JC estimate represents contributions from outside of the domain. However, comparing both background subtractions gives us an idea of the impact of differences between background estimates, such as their variability.

2.3.5 Sensitivity to the Atmospheric Model

As discussed in Section 2.2, in this study we use the NAME atmospheric transport model. Although NAME has been extensively inter-compared to other transport models in several publications (e.g. Brunner et al., 2017; Rigby et al., 2019; Monteil et al., 2020), systematic errors in NAME will influence the comparison with observations. Whilst an extensive model inter-comparison exercise is beyond the scope of this paper, to provide a simple comparison with another widely used modelling system, we compare the NAME fossil fuel CO_2 time series to that of CarbonTracker Europe (CTE2022, van der Laan-Luijckx et al., 2017; Friedlingstein et al., 2022). CTE2022 uses the TM5 transport model (Krol et al., 2005) driven by ERA-5 meteorology to transport prior fluxes globally, and surface CO_2 fluxes are optimized on a weekly timestep over the period 2000–2021.
270 The prior fluxes are from the SiB4 biosphere model (Haynes et al., 2019), GFAS fire emissions (Kaiser et al., 2012), GridFED fossil fuel emissions (Jones et al., 2021) and JC ocean fluxes. CO_2 mole fractions based on the optimized CTE2022 at WAO are used here, with separate tracers are available for each of the described flux components.

2.4 Fossil fuel CO_2 mole fraction

275 Previous studies have indicated that we can assume that ocean fluxes do not contribute strongly to the overall APO at a measurement site over short time scales (Pickers, 2016; Pickers et al., 2017; Chevalier and WP4 CHE partners, 2021). Based on this assumption, it has been proposed that we can estimate regional $ffCO_2$ mole fractions from APO, following Pickers (2016):

$$ffCO_2 = \frac{\delta APO - \delta APO_{bg}}{R_{\delta APO:CO_2}} \quad (12)$$

280 where APO_{bg} is a background APO estimate, and $R_{\delta APO:CO_2}$ is the APO: $ffCO_2$ ratio which can be estimated from $R_{APO:CO_2} = \alpha_f - \alpha_B$.



To estimate the time-varying ratio $R_{\delta APO:CO_2}$ in the air intercepted at the measurement site, we use the footprint-weighted fossil fuel exchange ratio:

$$R_{t,\delta APO:CO_2} = \frac{1}{\sum_{j=0}^n f_{p_{t,j}}} \sum_{j=0}^n (\alpha_{F_{t,j}} - \alpha_B) f_{p_{t,j}} \quad (13)$$

285 where t is the time, j is the grid cell and n is the maximum number of grid cells, $\alpha_{F_{t,j}}$ is α_F for one grid cell at that time, $f_{p_{t,j}}$ is one grid cell of the hourly footprint at that time, and $\sum_{j=0}^n f_{p_{t,j}}$ is the sum of the footprint across all grid cells at that time.

Here we investigate how well we can retrieve ffCO₂ mole fraction contributions from our APO models and we also estimate ffCO₂ from our observation using Equation 12. These estimates are directly compared to modeled ffCO₂ by multiplying the NAEl-within-EDGAR flux by NAME footprints, as described in Section 3.1. Equation 12 requires an estimate of the APO
 290 background, δAPO_{bg} . When deriving ffCO₂ from the model we compare two methods to estimate this term: in one case by fitting a baseline to the APO model using the REBS statistical fitting routine; for comparison we use the adjusted JC background estimate. The baselines for the whole of 2015 are shown in Supplementary Figure S9. We then derive ffCO₂ from the below-baseline APO, comparing the effect of using of a constant value for $R_{\delta APO:CO_2}$ and that using Equation 13 to calculate a time varying exchange ratio.

295 3 Results and discussion

3.1 Simulated APO at UK measurement sites

Here we show our APO model results for 2015. As examples, one summer (August) and one winter month (December) are shown throughout, and simulations for all months of 2015 and 2021 are provided in the Supplement (Figures S3 and S6).

The simulated CO₂ and O₂ mole fraction and APO contribution due to each source and sink is shown in Figure 4 for August
 300 and December 2015 at the three sites. In August, the ocean and fossil fuel mole fraction contributions have similar magnitudes and there are sustained periods during which the ocean APO component dominates over the fossil fuel. We find that there are O₂ excursions from background which are considerably larger than those inferred by Pickers et al. (2017). However, there is large disagreement between the three models of ocean APO contribution, and frequently the difference between them is of a similar magnitude to that of their contribution. Whereas over the summer the ED and JC models suggest net oxygen release
 305 from the ocean, over the winter we see overall uptake due to the difference in temperature and solubility, as well as the balance of respiration and productivity. In December, the magnitude of the fossil CO₂ and O₂ mole fractions are significantly larger than that of the ocean, although there are still large differences between the ocean models. However, when converted to the fossil fuel and ocean components of APO, the magnitudes are similar for Weybourne and for much of December the fossil fuel component is small compared with the ocean at Heathfield and Ridge Hill, despite these sites being further inland than
 310 WAO. For all three sites, variation between the ocean models is comparable to the magnitude of their flux and there are large periods of December during which the ocean is dominant as an O₂ sink. This is in contrast to the findings of Chevalier and

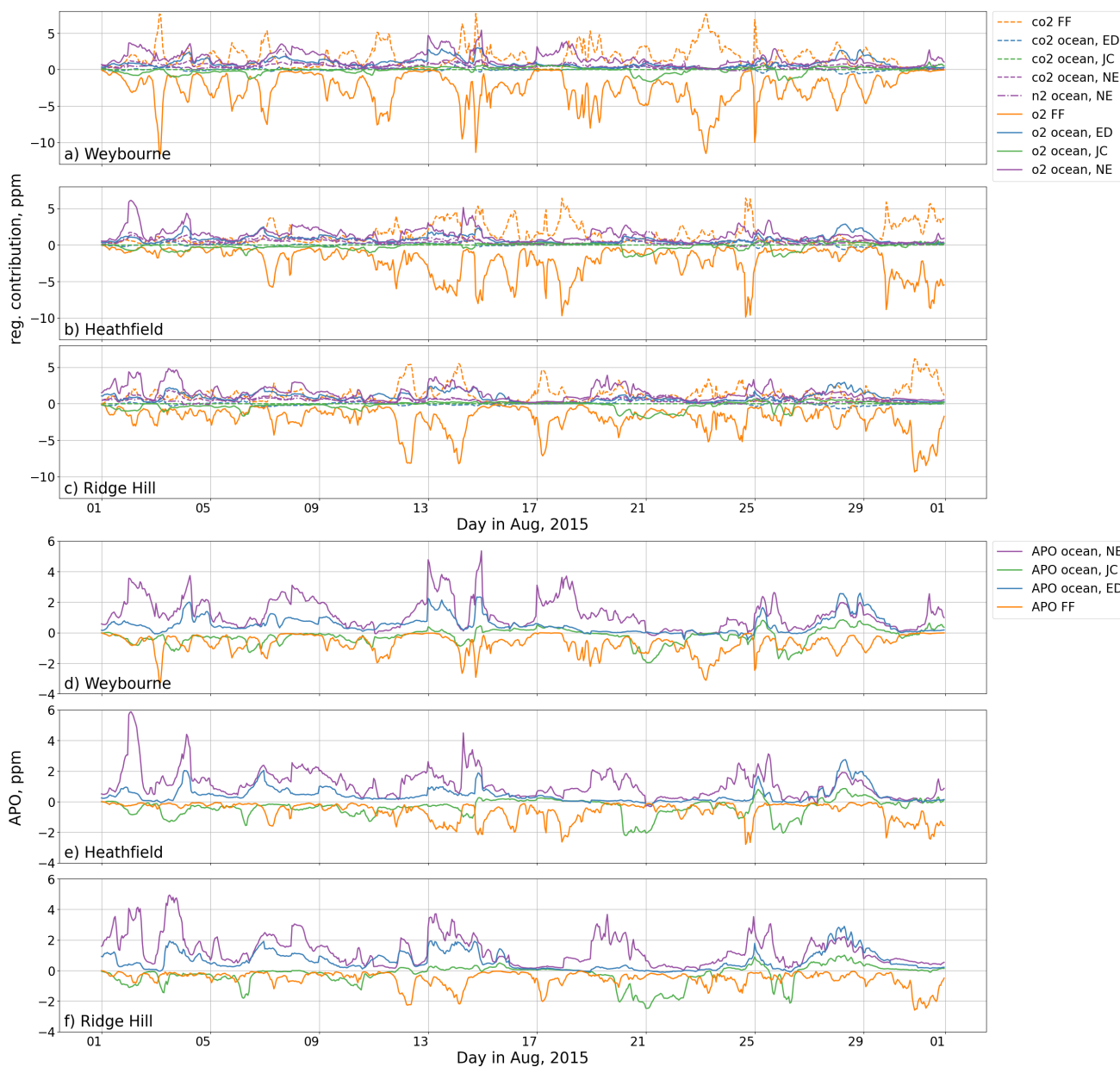


Figure 4. The regional contribution of the ocean and fossil fuel components of APO to the mole fraction of each species at Weybourne, Heathfield, and Ridge Hill (panels a, b, and c) and the overall regional ocean and fossil fuel contribution to the APO model at the three sites (panels d, e, and f) throughout August 2015. The blue, green, and purple line show the contribution calculated from the ED, JC, and NE fluxes respectively, and the orange lines show the fossil fuel contributions. Solid lines represent O₂ in the top panels and APO in the bottom panels, dashed lines show the CO₂, and dash-dotted lines show the N₂.

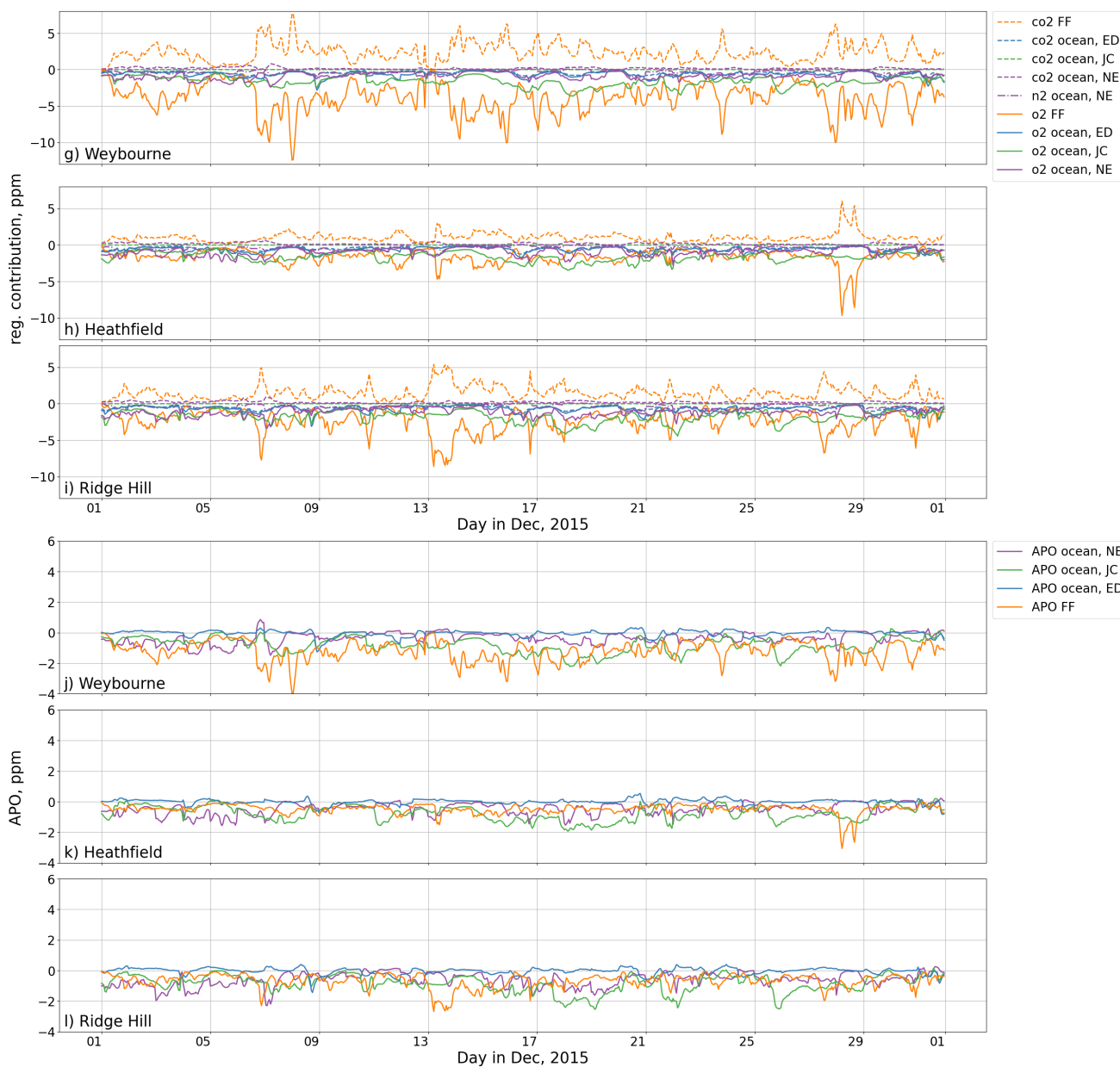


Figure 4. continued: the regional contribution of the ocean and fossil fuel components of APO to the mole fraction of each species at Weybourne, Heathfield, and Ridge Hill (panels *g*, *h*, and *i*) and the overall regional ocean and land contribution to the APO model at the three sites (panels *j*, *k*, and *l*) throughout December 2015. The blue, green, and purple line show the contribution calculated from the ED, JC, and NE fluxes respectively, and the orange line show the fossil contributions. Solid lines represent O₂ in the top panels and APO in the bottom panels, dashed lines show the CO₂, and dash-dotted lines show the N₂.

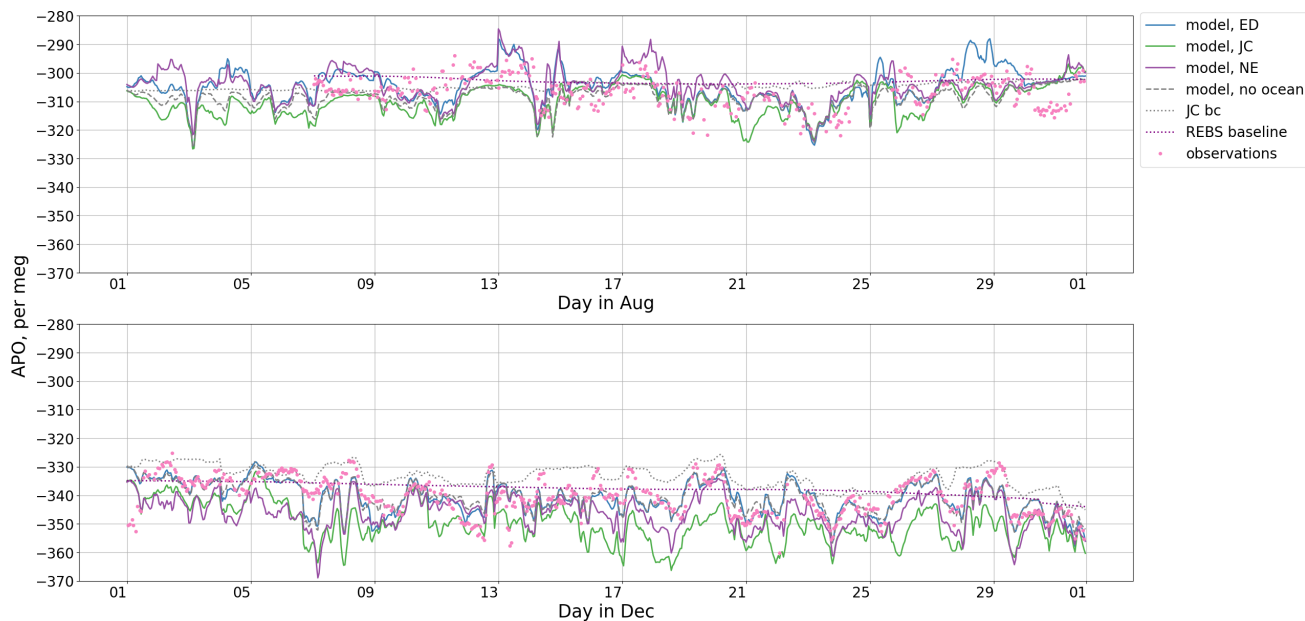


Figure 5. The modelled and observed APO at Weybourne throughout August (*panel a*) and December (*panel b*) 2015, where we model APO using three different ocean flux estimates from: the global ED ocean model (blue), the global JC inversion (green), and the regional NE ocean model (purple). We also show the APO model with no ocean contribution (grey dashed line). The dotted grey line shows the baseline derived from JC boundary conditions, which has been adjusted as described in Section 2.2.3. The magenta dots show the observations and the purple dotted line shows the baseline fit to the observations using the statistical fitting routine REBS.

WP4 CHE partners (2021), who found that the fossil fuel APO contribution was dominant at all sites, including Weybourne and Heathfield. That study used a combination of fluxes from NEMO–PlankTOM5 and the atmospheric transport model STILT (Lin et al., 2003). However, Chevalier and WP4 CHE partners (2021) do not provide details on the magnitude of variability in these flux estimates.

Combining the APO components using Equation 5 gives a modelled APO for Weybourne as shown in Figure 5 (for all three sites in 2015 see Supplementary Figure S3, and for Weybourne and Heathfield in 2021 see Supplementary Figure S6). Comparing with the observations we find that, although the magnitude of the variability is similar, there are substantial differences between the simulations and the observations. Figure 6 shows the (R^2) and root mean squared error (RMSE), comparing each model and the observations at Weybourne for each month throughout 2015. The APO model for December gives a closer fit to the observations at Weybourne than the model in August (average R^2 of 0.24 vs 0.10 and average RMSE of 6.7 vs 9.9 per meg for December and August, respectively). We see a clear seasonal trend, that the correlation is lowest throughout the summer and winter and increased during the spring and autumn. This is demonstrated further in Supplementary Figure S4, where there is larger scatter over the summer months. As discussed above and shown in Figure 5, we also find that the model is more sensitive to the ocean flux over the summer, when the difference between the three APO simulations using different

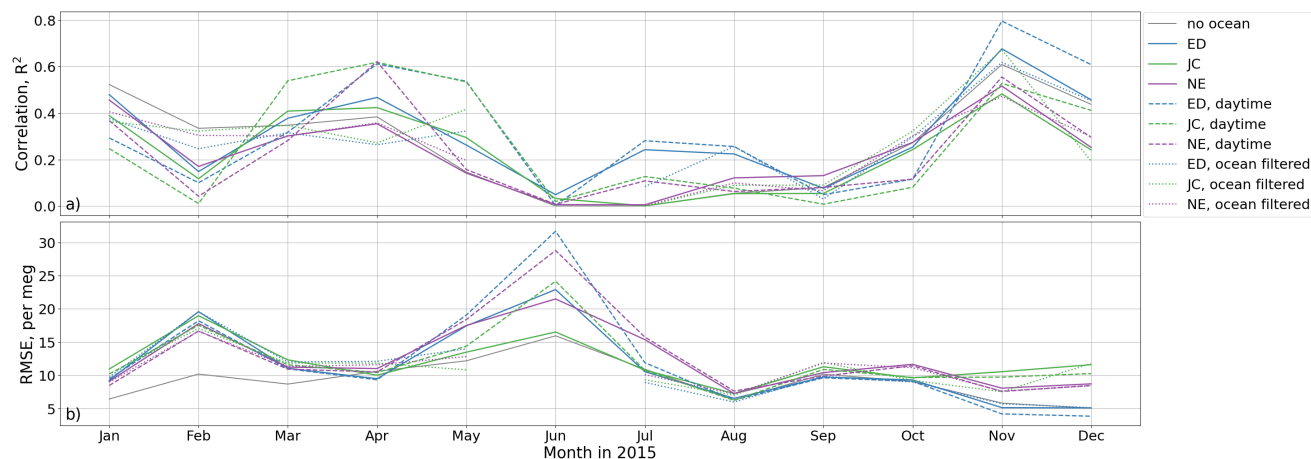


Figure 6. R^2 (panel a) and the root mean squared error (RMSE, panel b) of the modelled APO, compared with the observations at Weybourne in 2015. The blue, green, purple, and grey lines show the results from the models derived using the NAME simulations and either ED, JC, NE, and or no ocean fluxes, respectively. The solid, dashed, and dotted lines respectively show the correlations when we do not apply any filter, and when we filter for just daytime hours, and for times when the footprint has at least 40 % sensitivity to the land.

ocean fluxes is substantially larger (a monthly average of 7.0 per meg difference between the smallest and largest estimate in August, compared with 3.8 per meg in December). However, although our model agreement may be affected by ocean fluxes, we do not see a substantially better or worse fit when we exclude the ocean fluxes entirely, as shown in Figure 6. The R^2 and RMSE for the CO_2 and O_2 models are shown in Figure S5 of the Supplement, where we generally see higher correlations with the data for the CO_2 and O_2 simulations (R^2 generally above 0.4) than we do for APO. We also find that our 2021 model, shown in Figure S6 in the Supplement, does not display such large variability. In that simulation, we use ocean climatologies, finding that localised ocean emission or uptake events are smoothed as they are averaged across a number of years.

Next we try filtering our model in two ways to see the effects on the correlation with the observations. First we study only daytime hours (between 11:00 and 15:00), as the boundary layer is generally more well-mixed during the day than at night and so it is often assumed that the model-data mismatch will be smaller. Separately, we filter for times at which the footprint has at least 40 % sensitivity to the land, to investigate the effects of reducing the influence of ocean-dominated time steps. With both tests we see a small improvement in the correlation in some months, although overall, the difference with the simulations with no filtering is small (Figure 6). We further discuss the sensitivity to the ocean fluxes in Section 3.4.

3.2 Sensitivity to exchange ratios

The $3\text{-}\sigma$ sensitivity of APO to α_B and α_F is shown in the top and bottom panels of Figure 7, respectively ($3\text{-}\sigma$ is shown so that changes can be readily seen). In general, the model is more sensitive to α_F than α_B (average $1\text{-}\sigma$ interval of 0.27 and 0.41 per meg for α_B in August and December 2015 respectively, compared to 0.30 and 0.52 per meg for α_F). For both variables,

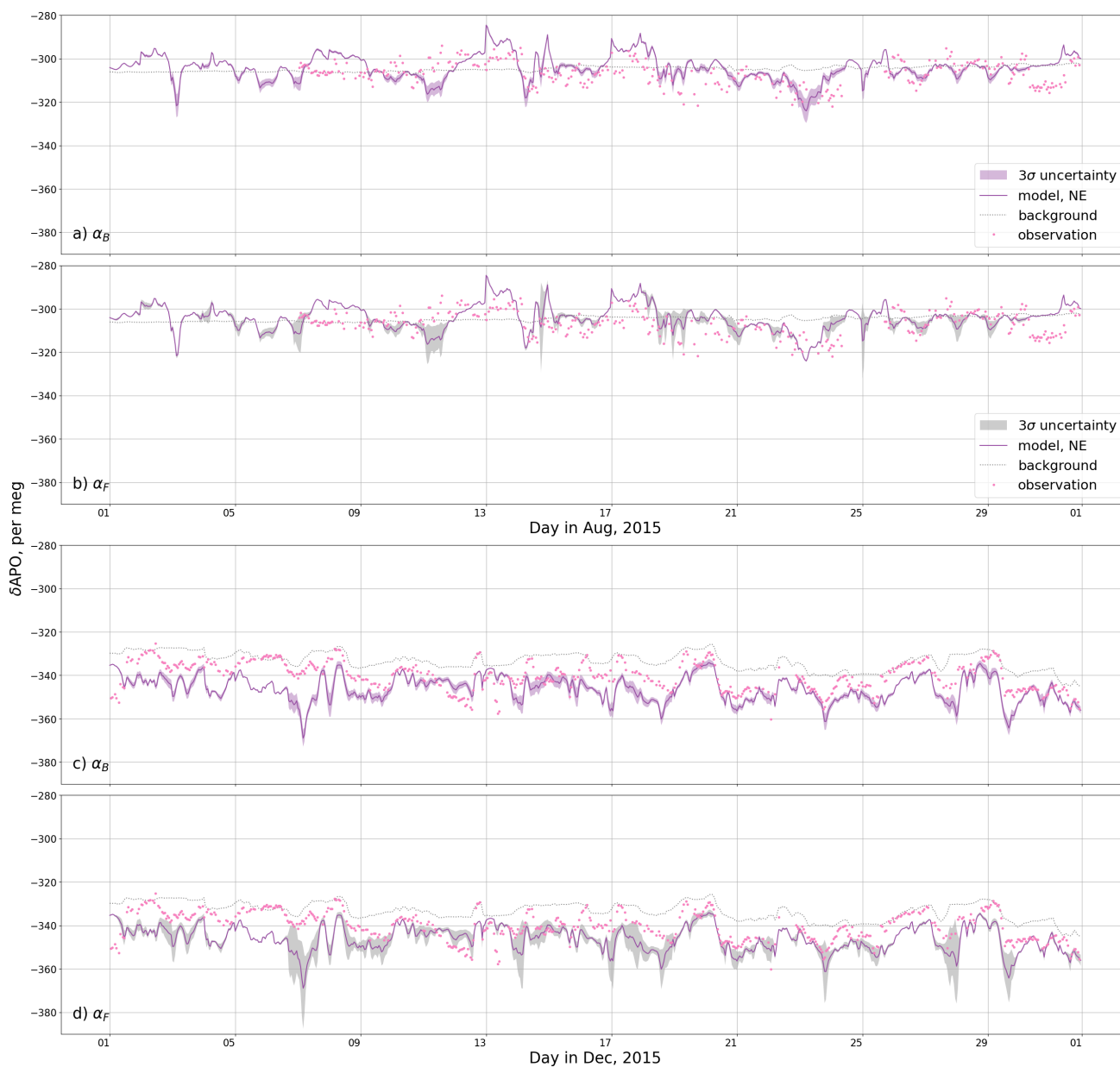


Figure 7. The APO at Weybourne during August (panels a and b) and December 2015 (panels c and d) and the sensitivity to α_B and α_F . The magenta points are the observations, the purple line is the model using NE ocean O_2 fluxes, and the shaded region is the three σ range derived from a Monte Carlo ensemble in which α_B (purple, panels a and c) and α_F (grey, panels b and d) are sampled.



	August 2015			December 2015		
	NAEI	EDGAR	NAEI-GridFED	NAEI	EDGAR	NAEI-GridFED
NAEI		0.957	0.999		0.910	0.994
EDGAR	0.957		0.962	0.910		0.911
NAEI-GridFED	0.999	0.962		0.994	0.911	

Table 1. R^2 for August and December 2015, comparing the modelled APO using NAEI CO₂ fluxes and exchange ratios, EDGAR CO₂ fluxes with GridFED exchange ratios, and NAEI CO₂ fluxes with GridFED exchange ratios. For these APO models we use the NE O₂ ocean flux estimates.

the influence on APO of a 1- σ change is generally small compared with the difference between the observations and the model that we see in Figure 5. We see larger sensitivity to both values of α when the mole fraction is dominated by fossil fuel fluxes.

345 3.3 Sensitivity to fossil fuel CO₂ flux

Figure 8 shows APO at Weybourne, with fossil fuel sources modelled using a combination of fluxes and exchange ratios as follows: NAEI (within EDGAR) with NAEI exchange ratios (labeled “NAEI”), EDGAR with GridFED exchange ratios (“EDGAR-GridFED”), and NAEI with GridFED exchange ratios (“NAEI-GridFED”). We find that, although there are variations in the magnitude at some time steps, the variability of the EDGAR and NAEI fossil fuel APO models is very similar.

350 For the most part, the two models agree, with high R^2 in both August and December 2015, as shown in Table 1. This suggests that the choice of inventory does not have a significant impact on the simulations compared with the other components that we investigate. Additionally, in agreement with the findings of section 3.2, the model does not seem highly sensitive to α_F : the application of different fossil fuel exchange ratios to estimate the O₂ uptake does not cause strong disagreement between the two fossil fuel O₂ models in Figure 8, which have a high R^2 .

355 Figure 8 shows the modelled APO timeseries and the associated 3- σ range when sampling fossil fuel emissions magnitude with a 10% standard deviation. The sensitivity is highest when the air comes from populated areas. However, these periods of high sensitivity do not necessarily coincide with times when the discrepancy between the model and observations is highest, suggesting that errors in fossil fuel fluxes alone could not explain some of the differences between the model and observations.

3.4 Sensitivity to ocean flux

360 When comparing APO models and observations in Figure 6 (and Figures S3 and S4 of the Supplement), we find the biggest disagreement during the summer. At this time of year there is increased ocean productivity compared to over the winter, thus the variations between the models are larger and the APO models vary more widely. Conversely, the highest correlation between all models and the observations is seen in October (see Figure S7 of the Supplement), when the ocean acts as a small O₂ sink, and the O₂ ocean flux is smallest of any month. We see in Figures 4, 5, and Supplementary Figure S3 that the models using
 365 the ED and NE fluxes exhibit large events of O₂ release throughout the summer, which are more exaggerated in NE. At some

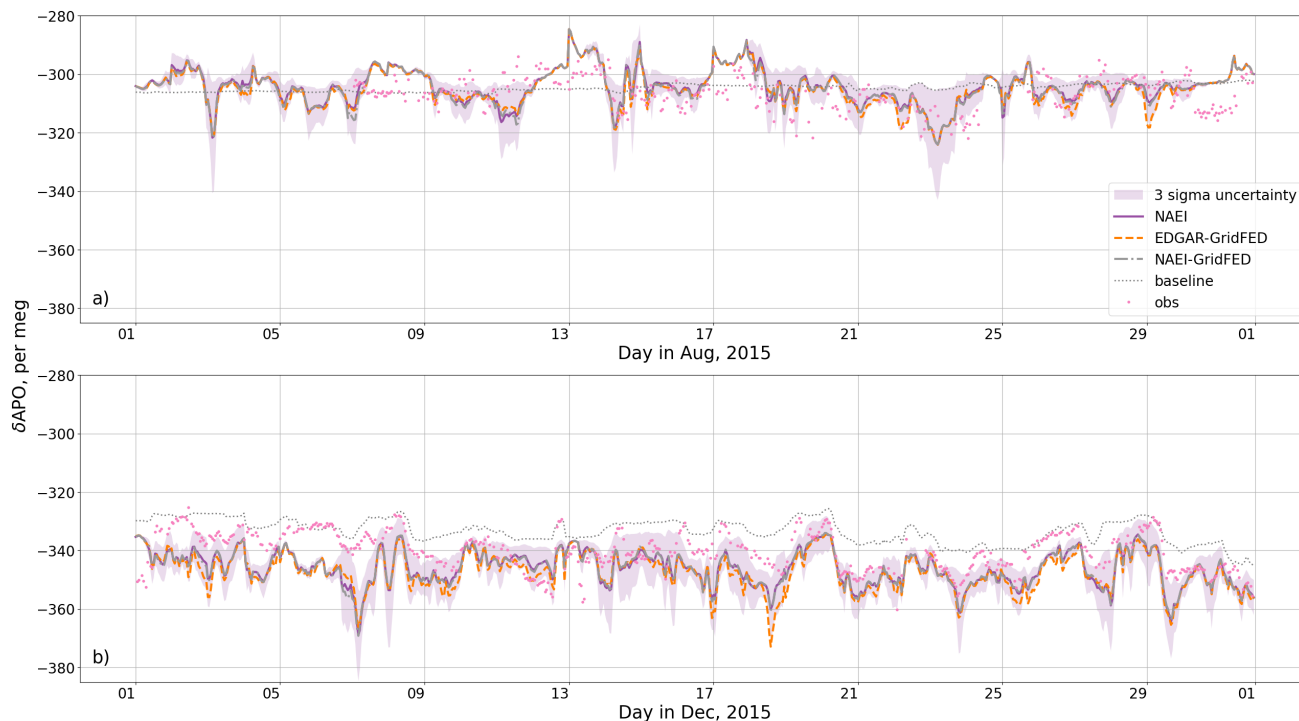


Figure 8. The APO model at Weybourne in August (*panel a*) and December (*panel b*) 2015 using NAME footprints and O₂ fluxes from the NE ocean model, comparing the model using with NAEI fluxes and exchange ratios (purple), with that using NAEI fluxes and GridFED exchange ratios (grey), and that using EDGAR fluxes and GridFED exchange ratios (orange). The observations are shown in magenta, the shaded regions represent the 3 σ uncertainty in the model assuming a 10 per cent 1 σ uncertainty on the fossil fuel component, and the grey dotted line is the background derived from JC boundary conditions.

of these times we see large differences between the ED and NE models compared with the model with no ocean component, as the ocean models indicate large APO excursions. Between April and June especially there are excursions in the NE APO model which have a much larger magnitude (up to ~ 85 per meg) than any in the observations. On the other hand, JC shows much smaller O₂ fluxes with generally smoother variations, and even suggests some negative APO contribution from the ocean during the summer. At some points during the summer we therefore see increased variability with NE compared with the other models. This difference may be due to the handling of coastal fluxes and the influence of rivers, which are more finely resolved in NE with its higher spatial resolution (~ 7 km vs ~ 18 km), and explicit nutrient input from rivers, and by a more detailed representation of phytoplankton physiological processes (e.g. variable stoichiometry). Another factor that could contribute to the differences between the estimates of O₂ air-sea fluxes between the ocean models is the differences in the wind products used to drive the air-sea exchange and their spatial and temporal resolution.

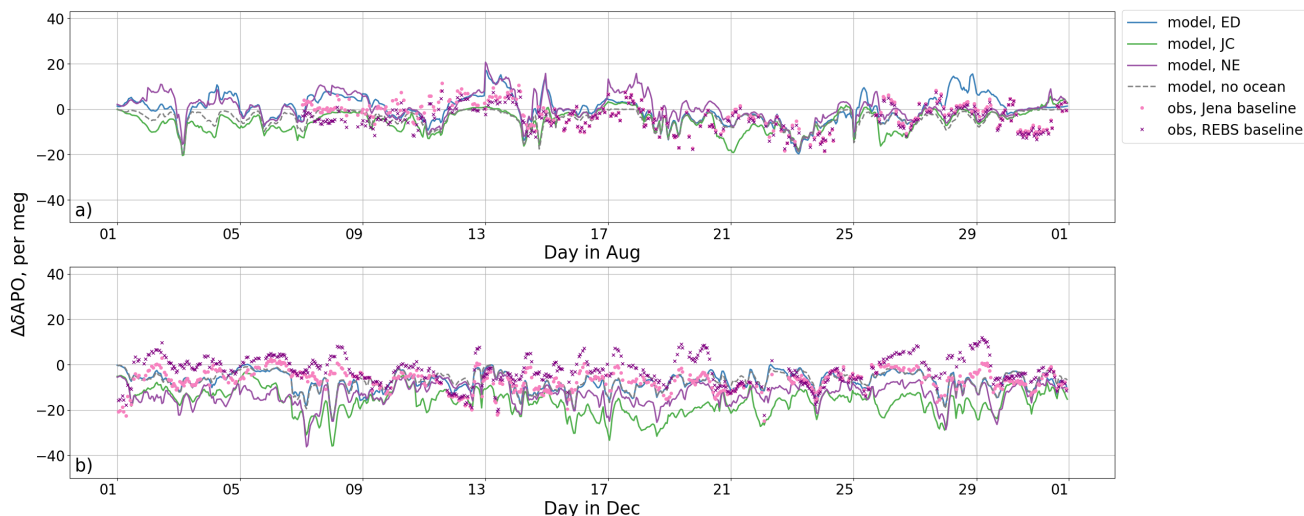


Figure 9. The modelled regional APO contribution and the background-subtracted APO observations at Weybourne throughout August (*panel a*) and December (*panel b*) 2015, where we model APO using three different ocean flux estimates from: the global ED ocean model (blue), the global JC inversion (green), and the regional NE ocean model (purple). We also show the APO model with no ocean contribution (grey line). We show two versions of background subtraction using a statistical routine (REBS, purple crosses), and using the JC background (pink points).

Based on our investigation we cannot determine which, if any, of the ocean flux estimates best represent the APO contribution to sites in the UK on average, although there may be some events during the summer in the NE and ED simulations that are inconsistent with the data. Furthermore, we do not see a substantial difference in correlation between the observations and either the simulations that include ocean fluxes or that which does not.

380 3.5 Sensitivity to the background estimate

Figure 9 shows the modelled regional $\Delta(\delta\text{APO})$ and the background-subtracted observations. We compare the background subtraction from the statistical (REBS) filter with the adjusted model-estimated baseline from the JC global fields. For most of the time series, the two baseline estimates lead to similar regional signals. In December there is more of a difference between the two signals, where at some regions the REBS subtracts a smaller background and leaves positive APO excursions. We expect that this difference arises because there is more variability within the JC background estimate. We saw in Figure S2 of the Supplement that this variability is increased in the winter compared to summer. We see in Figure 10 that the correlation between the background-subtracted observations and the models is similar for both methods of background subtraction. Neither choice leads to a substantial difference in model-data mismatch.

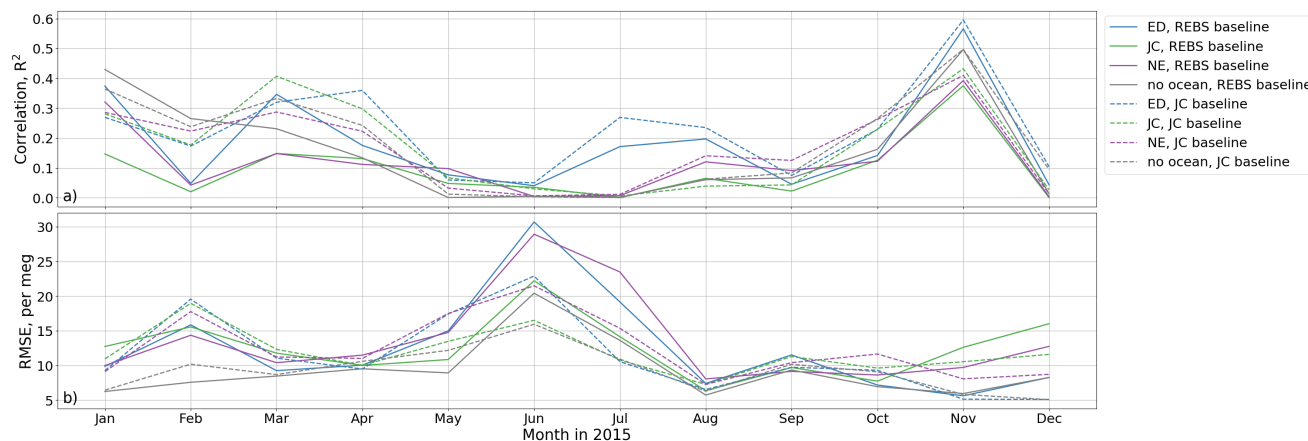


Figure 10. The square of the Pearson correlation coefficient (R^2 , *panel a*) and the RMSE (*panel b*) of the modelled regional contribution of APO, compared with the background subtracted observations at Weybourne in 2015. The blue, green, purple, and grey lines show the results from the models derived using the NAME simulations and either ED, JC, NE, or no ocean fluxes respectively. The solid and dashed lines respectively show the results when we subtract the REBS statistical background from the observations, and when we subtract the JC derived background.

3.6 Estimation of fossil fuel CO_2

390 Here we test how well we can retrieve the regional contribution of ffCO_2 from our modelled APO, using the method described in Section 2.4. Figure 11 and Supplementary Figure S10 show the comparison between ffCO_2 derived from our modelled APO and the direct simulation of ffCO_2 using NAME (i.e., ffCO_2 fluxes multiplied by NAME footprints). The comparison for all months throughout 2015 and the correlations are shown in Supplement Figure S10. Comparisons are shown when three different ocean flux estimates are used, or two different methods for subtracting the baseline. Differences between the APO-
 395 derived ffCO_2 and the direct ffCO_2 simulation will be due to the influence of ocean fluxes on the APO simulation (which is assumed negligible in Equation 12) and mis-specification of the background. All other factors, including atmospheric transport, are consistent between the two sets of simulations. Therefore, the APO-derived ffCO_2 using the adjusted JC background exactly matches the direct ffCO_2 simulation, if ocean fluxes are zero.

Firstly, we will consider the APO-derived ffCO_2 using the adjusted JC backgrounds. Throughout the summer, when there
 400 are large O_2 release events in the modelled ocean fluxes, the APO simulation using NE generally underestimates ffCO_2 , even indicating negative mole fractions for large parts of the month. The ED and JC APO simulations show closer overall agreement with ffCO_2 in August, although some discrepancy remains for all three. All three models overestimate the ffCO_2 for the majority of the winter compared to the direct ffCO_2 simulation. In this case the background APO, estimated as described in Section 2.4, is underestimated for large parts of the month, which may be due to modelled oceanic uptake of oxygen around the
 405 UK throughout the winter. Chevalier and WP4 CHE partners (2021) found high correlations between their APO-derived ffCO_2

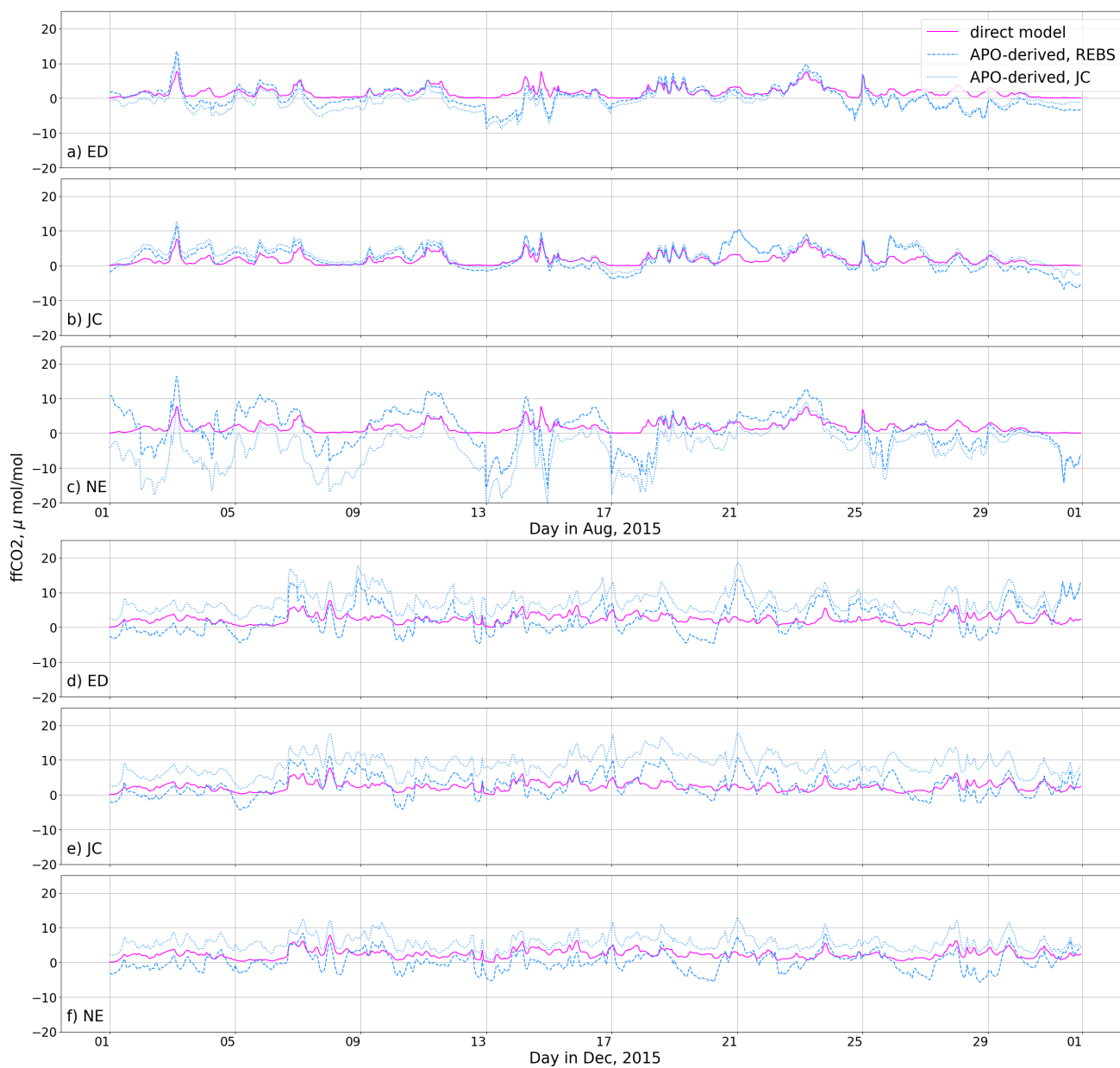


Figure 11. The modelled $ffCO_2$ for August (panels *a*, *b*, and *c*) and December (panels *d*, *e*, and *f*) 2015 derived from the APO model for Weybourne using the results from three different ocean flux fields (blue): ED (panels *a* and *d*), JC (panels *b* and *e*), and NE (panels *c* and *f*). We compare with the model calculated directly from the NAEI-within-EDGAR fluxes and NAME footprints (pink). The direct model is equivalent to the $ffCO_2$ in the top panels of Figure 4 and the APO models are shown in Figure 5.



and direct STILT model. However, it is unclear from that work as to the time period over which this correlation was found, and it should be noted that our correlation is greatly improved when averaging over larger time periods, due to the seasonality in APO.

For the simulations in which the REBS baseline has been fit to the APO simulations and then subtracted, the derived ffCO_2 from ED and NE is higher during the summer and lower during the winter than when the adjusted JC background is used. For the model that used JC ocean fluxes, which are considerably smaller than either ED or NE, there is a much smaller difference between the two estimates. The large difference between the simulations using these two baseline estimates likely stems from the influence of ocean fluxes. The REBS fit incorporates seasonal oceanic trends and thus removes large-timescale oceanic fluxes from the model. However, it is also susceptible to fitting to large APO excursions in the model which occur due to modelled short-term variability from the ocean, this is particularly clear throughout June in Figure S9 of the Supplement. On the other hand, as JC is independent of the model it does not encapsulate any regional ocean influence, and any ocean contribution is treated as ffCO_2 .

In Section 2.4 we make the assumption that the ocean component of the APO measurements is negligible when deriving ffCO_2 . This is based on previous studies of short-term ocean-related APO variability, which in turn are based on observations. Yet these models all indicate a persistent ocean contribution at all sites, which biases our calculation of ffCO_2 from the APO simulations. As shown in Section 3.1, there is large variation in O_2 flux estimates between ocean models. However, we cannot conclude which model, if any, gives a more accurate representation of the ocean O_2 flux. Furthermore, the CO_2 and O_2 ocean fluxes are decoupled and therefore, the exchange ratio varies as the footprint intercepts different parts of the ocean. Based on our analysis using these three ocean flux estimates, a correction for oceanic fluxes would be subject to substantial uncertainty.

Next we apply the same method to estimate ffCO_2 from the observed APO at Weybourne (Pickers et al., 2022) as described in Section 2.4. Figure 12 shows observation-derived ffCO_2 compared with the direct ffCO_2 simulations. Here, we have used the NAME simulation with NAEI and EDGAR fluxes, and also the outputs of the CTE system. The correlations (R^2) between the observation-derived ffCO_2 and the ffCO_2 model are shown in Figure 13. As we found in Section 2.2, we generally see low correlations over the summer, with stronger agreement in March, April, and November. There is not a large difference in the correlation for the JC and REBS background subtractions. This is contrary to our findings above shown in Figure 11, where we saw that there was sometimes large differences in ffCO_2 estimates for different methods of background subtraction due to the large ocean contribution which was assumed to be encapsulated in the background estimate. Throughout December we see that when using the REBS background subtraction we estimate frequent negative ffCO_2 contributions, which are not as apparent when subtracting the JC background, which may be a result of increased variability of the JC background estimate. Based on the synthetic data results presented in the previous paragraphs, discrepancies may be because of the influence of non-negligible ocean flux contributions, or errors in assigning baseline values. At some times we see a $\sim 5 - 8 \mu\text{mol/mol}$ difference between the direct model and the observation-derived ffCO_2 using the REBS background subtraction; this translates to an ocean contribution of $\sim 10 - 20$ per meg. This would be a large contribution, although the majority of the differences between the estimates are much smaller than this.

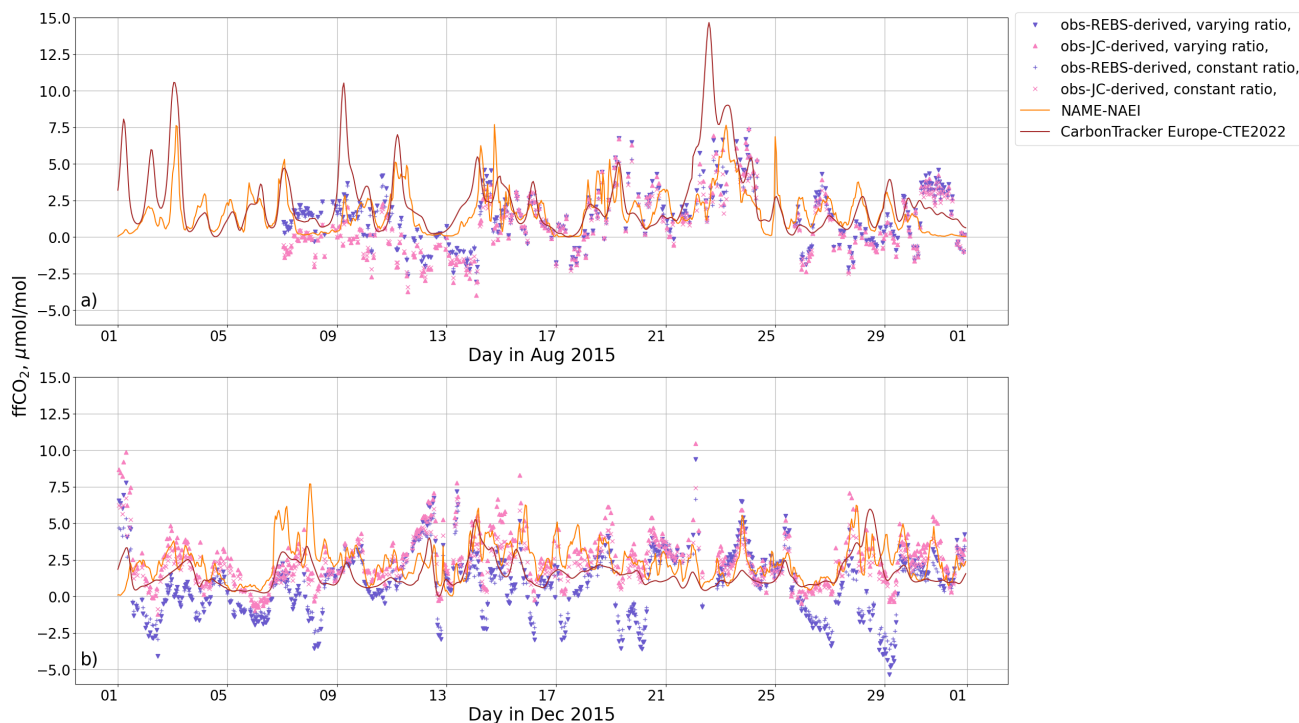


Figure 12. The regional contribution of ffCO_2 to the atmospheric abundance at Weybourne for August (*panel a*) and December (*panel b*) 2015. The pink triangles and crosses show the ffCO_2 model derived from the APO observations with the JC background subtracted using a time-varying and a constant exchange ratio respectively, the purple triangles and pluses show the same but with the REBS baseline subtracted, the orange line shows the model calculated directly from the NAEI-within-EDGAR fluxes and NAME footprints (equivalent to that in the top panels of Figure 4) and the brown line shows the model derived from CarbonTracker Europe (CTE2022).

440 We also test the conversion of the APO observations to ffCO_2 using a constant APO: ffCO_2 ratio, assuming $\alpha_F = -1.5$, as shown by the blue points in Figure 12. Throughout the year, the correlation between this estimate of ffCO_2 and the direct model are slightly lower than when using a time-varying APO: ffCO_2 ratio. Thus we find that using a time-varying APO: ffCO_2 ratio gives a slightly closer fit to the direct ffCO_2 simulation.

4 Future outlook

445 Improvements in the measuring and modelling of tracers are important for future evaluation of ffCO_2 emissions. Our investigation has shown that there are several inputs which can sometimes substantially change the modelled APO. In particular, a better understanding of oceanic CO_2 and O_2 fluxes in coastal regions seems to be the most important of the factors we tested, as such continental sites far from ocean influence may currently be more viable for APO models. We also saw that the choice

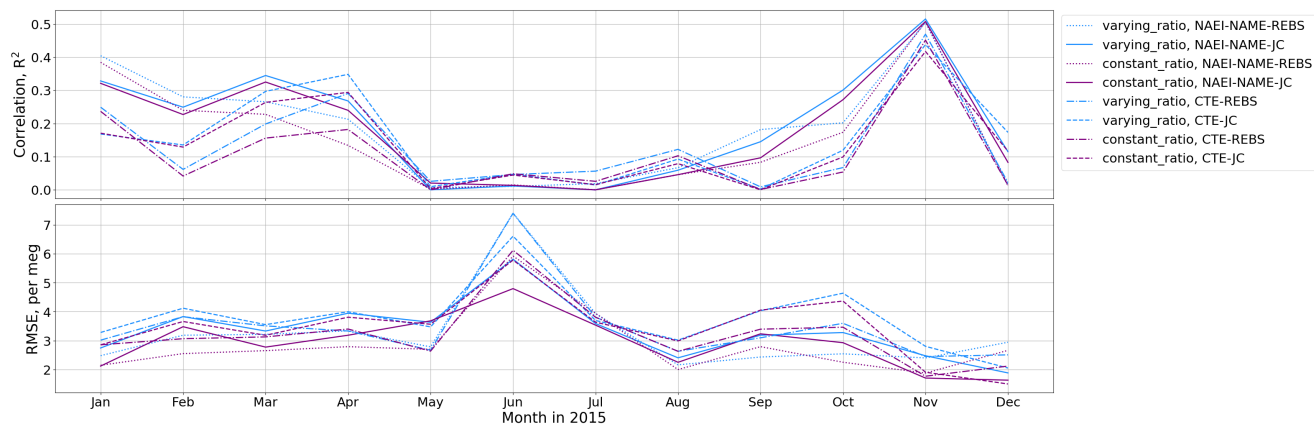


Figure 13. The square of the Pearson correlation coefficient (R^2 , *panel a*) and the root mean squared error (RMSE, *panel b*) of the modelled APO, compared with the observations at Weybourne in 2015. The blue and purple lines show the correlation when using a time-varying and constant APO:ffCO₂ ratio respectively, the solid lines show the correlation between the NAME-NAEI model and the JC-background-subtracted observations, and the dotted lines show the same but with the REBS-background-subtracted observations. The dashed lines show the correlation between the CTE model and the JC-background-subtracted observations, and the dash-dotted lines show the same but with the REBS-background-subtracted observations.

of baseline affects our APO model and derived ffCO₂, although errors in assigning regional baselines may also be due in part
450 to the influence of non-terrestrial fluxes.

Alongside APO, other tracers such as radiocarbon and CO can give extra insight into ffCO₂ emissions. Several studies have
shown that radiocarbon is a promising tool for this (e.g. Levin et al., 2003; Graven et al., 2009). However, unlike APO, most
radiocarbon programs rely on flask measurements which are not continuous and require time-consuming analysis. This makes
radiocarbon a comparatively expensive method which cannot presently provide such insight into high-frequency variability.
455 Radiocarbon measurements are also susceptible to contamination of emissions from the nuclear power industry, correcting for
which requires access to data which is not currently publicly available in the UK. Although CO measurement are much cheaper
than radiocarbon and can be made continuously (e.g. Andrews et al., 2014; Levin and Karstens, 2007; Levin et al., 2020), the
conversion from CO to ffCO₂ is uncertain.

Given the challenges of each, no one tracer currently provides the answer to the verification of ffCO₂ emissions. However,
460 we have identified key areas of focus which may improve the modelling of APO and its use as a ffCO₂ tracer.

5 Conclusions

We have simulated the tracer APO throughout the years 2015 and 2021 at three sites in the UK: Weybourne, Heathfield, and
Ridge Hill. Generally, the correlation with the observations is small for APO. We find large modelled ocean signals which



sometimes dominate the APO model, and that correlations tend to be higher for APO during the spring and autumn when
465 ocean fluxes are smallest.

We have presented a sensitivity analysis of the factors that most strongly influence modelled atmospheric APO. Our simu-
lations suggest that uncertainties in ocean fluxes contribute substantially to modelled APO and APO-derived ffCO₂ from the
model at measurement sites in the UK. Our analysis cannot determine which ocean model (or indeed, zero ocean flux) or base-
line estimation method leads to closest agreement the observations. However, a robust estimate of ffCO₂ is likely to depend
470 strongly on these factors being well known. In comparison, the sensitivity of atmospheric APO to uncertainties in fossil fuel
and terrestrial biosphere exchange ratios was relatively small. Our analysis shows that further work should focus on improving
ocean O₂ and CO₂ flux estimates to improve the accuracy of high-frequency APO-derived ffCO₂ in the UK.

6 Code Availability

The code for the analysis presented is available at https://github.com/hanchawn/APO_modelling (Chawner, 2023). We also
475 use code developed by the ACRG Modelling team at the University of Bristol, which is available at <https://github.com/ACRG-Bristol/acrg>.

7 Data Availability

The datasets generated and analysed during this study are available at <https://zenodo.org/record/7681834> (Chawner et al.,
2023). The observational datasets are available on CEDA at:

- 480
- Heathfield CO₂ and O₂: <https://catalogue.ceda.ac.uk/uuid/bfc2483537a744dca8e3239278b6e522>
 - Weybourne CO₂: <https://catalogue.ceda.ac.uk/uuid/87fc265aab6b4aeb961e62da2cd6ca91>
 - Weybourne O₂: <https://catalogue.ceda.ac.uk/uuid/b3f9714c956f428a840211e0184e23eb>

8 Author contribution

HC carried out the atmospheric modelling and data analysis with contributions from PAP, YA, AJM, CR, GL, PL and ITL.
485 Measurements were made by KEA and PAP, with support from TA, CD, GLF and CR. HC wrote the paper, with contributions
from MR, PAP, YA, ITL, HG, ALG and all co-authors.

9 Competing interests

The authors declare that they have no conflict of interest.



10 Acknowledgements

490 HC, MR and ALG were supported by a Natural Environment Research Council grant to the University of Bristol as part of the Detection and Attribution of Regional Emissions (DARE-UK) project, NE/S004211/1. We thank P. Wilson, and T. Barningham for assisting with maintaining the WAO O₂ and CO₂ measurement system during 2015.

Atmospheric O₂ and CO₂ measurements at WAO in 2015 and 2021 were funded by the U.K. Natural Environment Research Council (NERC) grants NE/I013342/1, NE/S004521/1, and NE/R011532/1. The WAO atmospheric O₂ and CO₂ measurements
495 have also been supported by the U.K. National Centre for Atmospheric Science (NCAS) from 1st December 2013 onward. P.A.P., K.E.A., and G.L.F. received funding from the NERC project DARE-UK (NE/S004211/1), and P.A.P and K.E.A. have received funding from the Horizon Europe project PARIS (101081430).

YA and GL acknowledge DARE-UK (NE/S004947/1) and the U.K. National Capability NERC Climate Linked Atlantic Sector Science program (NERC grant no. NE/R015953/1).



500 References

- Adcock, K. E., Manning, A. C., Pickers, P. A., Forster, G. L., Fleming, L., Barningham, T., and Wilson, P.: Continuous measurements of atmospheric CO₂, O₂ and APO at Weybourne Atmospheric Observatory, in prep.
- Andrews, A. E., Kofler, J. D., Trudeau, M. E., Williams, J. C., Neff, D. H., Masarie, K. A., Chao, D. Y., Kitzis, D. R., Novelli, P. C., Zhao, C. L., Dlugokencky, E. J., Lang, P. M., Crotwell, M. J., Fischer, M. L., Parker, M. J., Lee, J. T., Baumann, D. D., Desai, A. R., Stanier, C. O., De Wekker, S. F. J., Wolfe, D. E., Munger, J. W., and Tans, P. P.: CO₂, CO, and CH₄ measurements from tall towers in the NOAA Earth System Research Laboratory's Global Greenhouse Gas Reference Network: instrumentation, uncertainty analysis, and recommendations for future high-accuracy greenhouse gas monitoring efforts, *Atmospheric Measurement Techniques*, 7, 647–687, <https://doi.org/10.5194/amt-7-647-2014>, 2014.
- Barningham, T.: Detection and attribution of Carbon Cycle Processes from Atmospheric O₂ and CO₂ measurements at Halley Research Station, Antarctica and Weybourne Atmospheric Observatory, UK, Ph.D. thesis, University of East Anglia, 2018.
- Battle, M., Fletcher, S. M., Bender, M., Keeling, R. F., Manning, A. C., Gruber, N., Tans, P. P., Hendricks, M. B., Ho, D. T., Simonds, C., Mika, R., and Paplawsky, B.: Atmospheric potential oxygen: New observations and their implications for some atmospheric and oceanic models, *Global Biogeochemical Cycles*, 20, <https://doi.org/10.1029/2005GB002534>, 2006.
- Blaine, T. W., Keeling, R. F., and Paplawsky, W. J.: An improved inlet for precisely measuring the atmospheric Ar/N₂ ratio, *ACP*, 6, 1181–1184, 2006.
- Bozhinova, D., Palstra, S. W. L., van der Molen, M. K., Krol, M. C., Meijer, H. A. J., and Peters, W.: Three Years of $\Delta^{14}\text{CO}_2$ Observations from Maize Leaves in the Netherlands and Western Europe, *Radiocarbon*, 58, 459–478, <https://doi.org/10.1017/RDC.2016.20>, 2016.
- Brix, H., Menemenlis, D., Hill, C., Dutkiewicz, S., Jahn, O., Wang, D., Bowman, K., and Zhang, H.: Using Green's Functions to initialize and adjust a global, eddying ocean biogeochemistry general circulation model, *Ocean Modelling*, 95, 1–14, <https://doi.org/https://doi.org/10.1016/j.ocemod.2015.07.008>, 2015.
- Brunner, D., Arnold, T., Henne, S., Manning, A., Thompson, R. L., Maione, M., O'Doherty, S., and Reimann, S.: Comparison of four inverse modelling systems applied to the estimation of HFC-125, HFC-134a, and SF₆ emissions over Europe, *ACP*, 17, 10651–10674, <https://doi.org/10.5194/acp-17-10651-2017>, 2017.
- Butenschön, M., Clark, J., Aldridge, J. N., Allen, J. I., Artioli, Y., Blackford, J., Bruggeman, J., Cazenave, P., Ciavatta, S., Kay, S., Lessin, G., van Leeuwen, S., van der Molen, J., de Mora, L., Polimene, L., Saille, S., Stephens, N., and Torres, R.: ERSEM 15.06: a generic model for marine biogeochemistry and the ecosystem dynamics of the lower trophic levels, *Geoscientific Model Development*, 9, 1293–1339, <https://doi.org/10.5194/gmd-9-1293-2016>, 2016.
- Carroll, D., Menemenlis, D., Adkins, J. F., Bowman, K. W., Brix, H., Dutkiewicz, S., Fenty, I., Gierach, M. M., Hill, C., Jahn, O., Landschützer, P., Lauderdale, J. M., Liu, J., Manizza, M., Naviaux, J. D., Rödenbeck, C., Schimel, D. S., Van der Stocken, T., and Zhang, H.: The ECCO-Darwin Data-Assimilative Global Ocean Biogeochemistry Model: Estimates of Seasonal to Multidecadal Surface Ocean pCO₂ and Air-Sea CO₂ Flux, *Journal of Advances in Modeling Earth Systems*, 12, e2019MS001888, <https://doi.org/https://doi.org/10.1029/2019MS001888>, e2019MS001888 2019MS001888, 2020.
- Chawner, H.: <https://doi.org/10.5281/zenodo.7688294>, 2023.
- Chawner, H., Adcock, K. E., Arnold, T., Artioli, Y., Dylag, C., Forster, G. L., Ganesan, A., Graven, H., Lessin, G., Levy, P., Luijckx, I. T., Manning, A., Pickers, P. A., Rennick, C., Rödenbeck, C., and Rigby, M.: <https://doi.org/10.5281/zenodo.7681834>, 2023.



- Chevalier, F. and WP4 CHE partners: D4.4 Sampling Strategy for additional tracers, <https://www.che-project.eu/node/243>, 2021.
- Ciais, P., Manning, A. C., Reichstein, M., Zaehle, S., and Bopp, L.: Nitrification amplifies the decreasing trends of atmospheric oxygen and implies a larger land carbon uptake, *Global Biogeochemical Cycles*, 21, <https://doi.org/https://doi.org/10.1029/2006GB002799>, 2007.
- 540 Cullen, M.: The unified forecast/climate model, *Meteorological Magazine*, 122, 81–94, 1993.
- Friedlingstein, P., O’Sullivan, M., Jones, M. W., Andrew, R. M., Gregor, L., Hauck, J., Le Quéré, C., Luijkx, I. T., Olsen, A., Peters, G. P., Peters, W., Pongratz, J., Schwingshackl, C., Sitch, S., Canadell, J. G., Ciais, P., Jackson, R. B., Alin, S. R., Alkama, R., Arneeth, A., Arora, V. K., Bates, N. R., Becker, M., Bellouin, N., Bittig, H. C., Bopp, L., Chevallier, F., Chini, L. P., Cronin, M., Evans, W., Falk, S., Feely, R. A., Gasser, T., Gehlen, M., Gkritzalis, T., Gloege, L., Grassi, G., Gruber, N., Gürses, O., Harris, I., Hefner, M., Houghton, R. A., Hurtt, 545 G. C., Iida, Y., Ilyina, T., Jain, A. K., Jersild, A., Kadono, K., Kato, E., Kennedy, D., Klein Goldewijk, K., Knauer, J., Korsbakken, J. I., Landschützer, P., Lefèvre, N., Lindsay, K., Liu, J., Liu, Z., Marland, G., Mayot, N., McGrath, M. J., Metzl, N., Monacci, N. M., Munro, D. R., Nakaoka, S.-I., Niwa, Y., O’Brien, K., Ono, T., Palmer, P. I., Pan, N., Pierrot, D., Pockock, K., Poulter, B., Resplandy, L., Robertson, E., Rödenbeck, C., Rodriguez, C., Rosan, T. M., Schwinger, J., Séférian, R., Shutler, J. D., Skjelvan, I., Steinhoff, T., Sun, Q., Sutton, A. J., Sweeney, C., Takao, S., Tanhua, T., Tans, P. P., Tian, X., Tian, H., Tilbrook, B., Tsujino, H., Tubiello, F., van der Werf, G. R., Walker, 550 A. P., Wanninkhof, R., Whitehead, C., Willstrand Wranne, A., Wright, R., Yuan, W., Yue, C., Yue, X., Zaehle, S., Zeng, J., and Zheng, B.: Global Carbon Budget 2022, *Earth System Science Data*, 14, 4811–4900, <https://doi.org/10.5194/essd-14-4811-2022>, 2022.
- Graven, H. and Gruber, N.: Continental-scale enrichment of atmospheric $^{14}\text{CO}_2$ from the nuclear power industry: potential impact on the estimation of fossil fuel-derived CO_2 , *ACP*, 11, 12 339–12 349, <https://doi.org/https://doi.org/10.5194/acp-11-12339-2011>, 2011.
- Graven, H., Stephens, B., Guilderson, T., Campos, T., Schiel, D., Campbell, J., and Keeling, R.: Vertical profiles of biospheric and fossil 555 fuel-derived CO_2 and fossil fuel CO_2 : CO ratios from airborne measurements of $\Delta^{14}\text{C}$, CO_2 and CO above Colorado, USA, *Tellus B: Chemical and Physical Meteorology*, 61, 536–546, <https://doi.org/10.1111/j.1600-0889.2009.00421.x>, 2009.
- Graven, H., Fischer, M., Lueker, T., Jeong, S., Guilderson, T., Keeling, R., Bambha, R., Brophy, K., Callahan, W., Cui, X., Frankenberg, C., Gurney, K., LaFranchi, B., Lehman, S., Michelsen, H., Miller, J., Newman, S., Paplawsky, W., Parazoo, N., Sloop, C., and Walker, S.: Assessing fossil fuel CO_2 emissions in California using atmospheric observations and models, *Environ. Res. Lett.*, 13, 065 007, 560 <https://doi.org/10.1088/1748-9326/aabd43>, 2018.
- Gruber, N., Gloor, M., Fan, S.-M., and Sarmiento, J. L.: Air-sea flux of oxygen estimated from bulk data: Implications For the marine and atmospheric oxygen cycles, *Global Biogeochemical Cycles*, 15, 783–803, 2001.
- Hamme, R. C.: The solubility of neon, nitrogen and argon in distilled water and seawater, *Deep Sea Research*, 51, 1517–1528, 2004.
- Haynes, K. D., Baker, I. T., Denning, A. S., Wolf, S., Wohlfahrt, G., Kiely, G., Minaya, R. C., and Haynes, J. M.: Representing Grasslands 565 Using Dynamic Prognostic Phenology Based on Biological Growth Stages: Part 2. Carbon Cycling, *Journal of Advances in Modeling Earth Systems*, 11, 4440–4465, <https://doi.org/https://doi.org/10.1029/2018MS001541>, 2019.
- Jones, A., Thomson, D., Hort, M., and Devenish, B.: The U.K. Met Office’s Next-Generation Atmospheric Dispersion Model, NAME III, pp. 580–589, Springer US, https://doi.org/10.1007/978-0-387-68854-1_62, 2007.
- Jones, M. W., Andrew, R. M., Peters, G. P., Janssens-Maenhout, G., De-Gol, A. J., Ciais, P., Patra, P. K., Chevalier, F., and Quere, C. L.: 570 Gridded fossil CO_2 emissions and related O_2 combustion consistent with national inventories 1959–2018, *Nature Scientific Data*, 8, 2021.
- Kaiser, J. W., Heil, A., Andreae, M. O., Benedetti, A., Chubarova, N., Jones, L., Morcrette, J.-J., Razinger, M., Schultz, M. G., Suttie, M., and van der Werf, G. R.: Biomass burning emissions estimated with a global fire assimilation system based on observed fire radiative power, *Biogeosciences*, 9, 527–554, <https://doi.org/10.5194/bg-9-527-2012>, 2012.



- Keeling, R.: Measuring correlations between atmospheric oxygen and carbon dioxide mole fractions: A preliminary study in urban air, *J Atmos Chem*, 7, 153–176, <https://doi.org/10.1007/BF00048044>, 1988a.
- Keeling, R. F.: Development of an interferometric oxygen analyzer for precise measurement of the atmospheric O₂ mole fraction, 1988b.
- Keeling, R. F. and Severinghaus, J.: Atmospheric oxygen measurements and the carbon cycle, *The carbon cycle*, 6, 2000.
- Keeling, R. F. and Shertz, S. R.: Seasonal and interannual variations in atmospheric oxygen and implications for the global carbon cycle, *Nature*, 358, 723–727, <https://doi.org/https://doi.org/10.1038/358723a0>, 1992.
- Keeling, R. F., Najjar, R. P., Bender, M. L., and Tans, P. P.: What atmospheric oxygen measurements can tell us about the global carbon cycle, *Global Biogeochemical Cycles*, 7, <https://doi.org/https://doi.org/10.1029/92GB02733>, 1993.
- Kozlova, E. A. and Manning, A. C.: Methodology and calibration for continuous measurements of biogeochemical trace gas and O₂ concentrations from a 300-m tall tower in central Siberia, *Atmos. Meas. Tech.*, 2, 205–220, 2009.
- Kozlova, E. A., Manning, A. C., Kisilyakhov, Y., Seifert, T., and Heimann, M.: Seasonal, synoptic, and diurnal-scale variability of biogeochemical trace gases and O₂ from a 300-m tall tower in central Siberia, *Global Biogeochemical Cycles*, 22, <https://doi.org/https://doi.org/10.1029/2008GB003209>, 2008.
- Krinner, G., Viovy, N., de Noblet-Ducoudré, N., Ogée, J., Polcher, J., Friedlingstein, P., Ciais, P., Sitch, S., and Prentice, I. C.: A dynamic global vegetation model for studies of the coupled atmosphere-biosphere system, *Global Biogeochemical Cycles*, 19, <https://doi.org/https://doi.org/10.1029/2003GB002199>, 2005.
- Krol, M., Houweling, S., Bregman, B., van den Broek, M., Segers, A., van Velthoven, P., Peters, W., Dentener, F., and Bergamaschi, P.: The two-way nested global chemistry-transport zoom model TM5: algorithm and applications, *Atmospheric Chemistry and Physics*, 5, 417–432, <https://doi.org/10.5194/acp-5-417-2005>, 2005.
- Kuijpers, B., Peters, W., and van der Laan-Luijkx, I.: Oxygen as a tracer for fossil fuel CO₂ emission sources, 2018.
- Levin, I. and Karstens, U.: Inferring high-resolution fossil fuel CO₂ records at continental sites from combined (CO₂)-C-14 and CO observations, 59, 245–250, <https://doi.org/10.1111/j.1600-0889.2006.00244.x>, 2007.
- Levin, I., Kromer, B., Schmidt, M., and Sartorius, H.: A novel approach for independent budgeting of fossil fuel CO₂ over Europe by 14CO₂ observations, *Geophys. Res. Lett.*, 30, 2194, <https://doi.org/10.1029/2003GL018477>, 2003.
- Levin, I., Karstens, U., Eritt, M., Maier, F., Arnold, S., Rzesanke, D., Hammer, S., Ramonet, M., Vítková, G., Conil, S., Heliasz, M., Kubistin, D., and Lindauer, M.: A dedicated flask sampling strategy developed for Integrated Carbon Observation System (ICOS) stations based on CO₂ and CO measurements and Stochastic Time-Inverted Lagrangian Transport (STILT) footprint modelling, *Atmospheric Chemistry and Physics*, 20, 11 161–11 180, <https://doi.org/10.5194/acp-20-11161-2020>, 2020.
- Lin, J. C., Gerbig, C., Wofsy, S. C., Andrews, A. E., Daube, B. C., Davis, K. J., and Grainger, C. A.: A near-field tool for simulating the upstream influence of atmospheric observations: The Stochastic Time-Inverted Lagrangian Transport (STILT) model, *J. Geophys. Res.-Atmos.*, 108, 4493, <https://doi.org/10.1029/2002JD003161>, 2003.
- Lunt, M. F., Rigby, M., Ganesan, A. L., , and Manning, A. J.: Estimation of trace gas fluxes with objectively determined basis functions using reversible-jump Markov chain Monte Carlo, *Geosci. Model Dev*, 9, 3213–3229, <https://doi.org/10.5194/gmd-9-3213-2016>, 2016.
- Machta, L. and Hughes, E.: Atmospheric Oxygen in 1967 to 1970, *Science*, 168, 1582–1584, <https://doi.org/10.1126/science.168.3939.1582>, 1970.
- Madec, G. and NEMO System Team: NEMO ocean engine, <https://doi.org/10.5281/zenodo.1464816>, 2022.
- Manning, A., O’Doherty, S., Jones, A., Simmonds, P., and Derwent, R.: Estimating UK methane and nitrous oxide emissions from 1990 to 2007 using an inversion modeling approach, *JGR*, 116, 2011.

Manning, A. C. and Keeling, R. F.: Global oceanic and land biotic carbon sinks from the Scripps atmospheric oxygen flask sampling network, *Tellus B: Chemical and Physical Meteorology*, 58, 95–116, 2006.

615 Marshall, J., Nuñez Ramirez, T., and WP4 CHE partners: D4.3 Attribution Problem Configurations, <https://www.che-project.eu/node/243>, 2019.

Monteil, G., Broquet, G., Scholze, M., Lang, M., Karstens, U., Gerbig, C., Koch, F.-T., Smith, N. E., Thompson, R. L., Lujikx, I. T., White, E., Meesters, A., Ciais, P., Ganesan, A. L., Manning, A., Mischurow, M., Peters, W., Peylin, P., Tarniewicz, J., Rigby, M., Rödenbeck, C., Vermeulen, A., and Walton, E. M.: The regional European atmospheric transport inversion comparison, EUROCOM: first results on European-wide terrestrial carbon fluxes for the period 2006–2015, *Atmospheric Chemistry and Physics*, 20, 12 063–12 091, 620 <https://doi.org/10.5194/acp-20-12063-2020>, 2020.

Nightingale, P., Malin, G., Law, C., Watson, A., Liss, P., Liddicoat, M., Boutin, J., and Upstill-Goddard, R.: In situ evaluation of air-sea gas exchange parameterizations using novel conservative and volatile tracers., *Global Biogeochem. Cycles*, 14, 373–387, <https://doi.org/10.1029/1999GB900091>, 2000.

Pickers, P.: New applications of continuous atmospheric O₂ measurements: meridional transects across the Atlantic Ocean, and improved 625 quantification of fossil fuel-derived CO₂, Ph.D. thesis, School of Environmental Sciences of the University of East Anglia, 2016.

Pickers, P. A.: personal communication.

Pickers, P. A., Manning, A. C., Sturges, W. T., le Quéré, C., Mikaloff Fletcher, S. E., Wilson, P. A., and Etchells, A. J.: In situ measurements of atmospheric O₂ and CO₂ reveal an unexpected O₂ signal over the tropical Atlantic Ocean., *Global Biogeochem. Cycles*, 31, 1289–1305, 2017.

630 Pickers, P. A., Manning, A. C., Quéré, C. L., Forster, G. L., Lujikx, I. T., Gerbig, C., Fleming, L. S., and Sturges, W. T.: Novel quantification of regional fossil fuel CO₂ reductions during COVID-19 lockdowns using atmospheric oxygen measurements, *Science Advances*, 8, eabl9250, <https://doi.org/10.1126/sciadv.abl9250>, 2022.

Rigby, M. and Park, S. S. T., Western, L. M., Redington, A. L., Fang, X., Henne, S., Manning, A. J., Prinn, R. G., Dutton, G. S., Fraser, P. J., Ganesan, A. L., Hall, B. D., Harth, C. M., Kim, J., Kim, K.-R., Krummel, P. B., Lee, T., Li, S., Liang, Q., Lunt, M. F., 635 Montzka, S. A., Mühle, J., O’Doherty, S., Park, M.-K., Reimann, S., Salameh, P. K., Simmonds, P., Tunnicliffe, R. L., Weiss, R. F., Y., Y., and Young, D.: Increase in CFC-11 emissions from eastern China based on atmospheric observations, *Nature*, 569, 546–550, <https://doi.org/https://doi.org/10.1038/s41586-019-1193-4>, 2019.

Rödenbeck, C., Bakker, D., N. Metzl, A. O., Sabine, C., Cassar, N., Reum, F., Keeling, R., and Heimann, M.: Interannual sea–air CO₂ flux variability from an observation driven ocean mixed-layer scheme, *Biogeosciences*, 11, 4599 – 4613, 640 <https://doi.org/https://doi.org/10.5194/bg-11-4599-2014>, 2003.

Rödenbeck, C., Quéré, C. L., Heimann, M., and Keeling, R.: Interannual variability in oceanic biogeochemical processes inferred by inversion of atmospheric O₂/N₂ and CO₂ data, *Tellus B*, 60, 685–705, <https://doi.org/https://doi.org/10.1111/j.1600-0889.2008.00375.x>, 2008.

Rödenbeck, C., Zaehle, S., Keeling, R., and Heimann, M.: How does the terrestrial carbon exchange respond to inter-annual climatic variations? A quantification based on atmospheric CO₂ data, *Biogeosciences*, 15, 2481–2498, <https://doi.org/https://doi.org/10.5194/bg-15-2481-2018>, 2018. 645

Ruckstuhl, A. F., Henne, S., Reimann, S., Steinbacher, M., Vollmer, M. K., O’Doherty, S., Buchmann, B., and Hueglin, C.: Robust extraction of baseline signal of atmospheric trace species using local regression., *AMT*, 5, 2613–2624, 2012.



- Stanley, M., Grant, A., O'Doherty, S., Young, D., Manning, A., Stavert, A., Spain, T., Salameh, P., Harth, C., Simmonds, P., Sturges, W.,
and D.E. Oram, R. D.: Greenhouse gas measurements from a UK network of tall towers: technical description and first results, *AMT*, 11,
650 <https://doi.org/10.5194/amt-11-1437-2018>, 2018.
- Steinbach, J., Gerbig, C., Rödenbeck, C., Karstens, U., Minejima, C., and Mukai, H.: The CO₂ release and Oxygen uptake from Fossil Fuel
Emission Estimate (COFFEE) dataset: effects from varying oxidative ratios, *ACP*, 11, 6855–6870, [https://doi.org/10.5194/acp-11-6855-](https://doi.org/10.5194/acp-11-6855-2011)
2011, 2011.
- Stephens, B., Keeling, R., Heimann, M., Six, K., Murnane, R., and Caldeira, K.: Testing global ocean carbon cycle models using measure-
655 ments of atmospheric O₂ and CO₂ concentration, *GBC*, 12, 213–230, 1998.
- Stephens, B. B., Bakwin, P. S., Tans, P. P., Teclaw, R. M., and Baumann, D. D.: Application of a differential fuel-cell analyzer for measuring
atmospheric oxygen variations, *J. Atmos. Oceanic Technol.*, 24, 82–94, 2007.
- Tsagatakis, I., Richardson, J., Evangelides, C., Pizzolato, M., Pearson, B., Passant, N., Pommier, M., and Otto, A.: UK Spatial Emissions
Methodology: A report of the National Atmospheric Emission Inventory 2020, https://naei.beis.gov.uk/reports/reports?report_id=1082,
660 2022.
- van der Laan-Luijkx, I. T., van der Velde, I. R., van der Veen, E., Tsuruta, A., Stanislawski, K., Babenhauserheide, A., Zhang, H. F., Liu, Y.,
He, W., Chen, H., Masarie, K. A., Krol, M. C., and Peters, W.: The CarbonTracker Data Assimilation Shell (CTDAS) v1.0: implementation
and global carbon balance 2001–2015, *Geoscientific Model Development*, 10, 2785–2800, <https://doi.org/10.5194/gmd-10-2785-2017>,
2017.
- 665 Wanninkhof, R.: Relationship between wind speed and gas exchange over the ocean, *Journal of Geophysical Research: Oceans*, 97, 7373–
7382, <https://doi.org/https://doi.org/10.1029/92JC00188>, 1992.
- Weast, R. C. and Astle, M.: Chemical Rubber Company Press, 1982.
- Wenger, A., Pugsley, K., O'Doherty, S., Rigby, M., Manning, A., Lunt, M., and White, E.: Atmospheric radiocarbon measurements to
quantify CO₂ emissions in the UK from 2014 to 2015, *ACP*, 19, 14 057–14 070, 2019.
- 670 White, E., Rigby, M., Lunt, M., Smallman, T., Comyn-Platt, E., Manning, A., Ganesan, A., O'Doherty, A., Stavert, A., Stanley, K., Williams,
M., Levy, P., Ramonet, M., Forster, G., Manning, A., and Palmer, P.: Quantifying the UK's carbon dioxide flux: an atmospheric inverse
modelling approach using a regional measurement network, *ACP*, 19, 2019.
- Wilson, P.: Insight into the Carbon Cycle from Continuous Measurements of Oxygen and Carbon Dioxide at Weybourne Atmospheric
Observatory, UK, Ph.D. thesis, University of East Anglia, 2013.
- 675 WMO: 20th WMO/IAEA Meeting on Carbon Dioxide, Other Greenhouse Gases and Related Measurement Techniques (GGMT-2019),
https://library.wmo.int/index.php?lvl=notice_display&id=21758#.Y_Sh7a3P1D8, 2019.